Posiva

Working Report 2020-01

Modelling Solute Transport and Water-Rock Interactions in Discrete Fracture Networks

David Applegate, Pete Appleyard, Steven Joyce

June 2020

POSIVA OY
Olkiluoto
FI-27160 EURAJOKI, FINLAND
Phone (02) 8372 31 (nat.), (+358-2-) 8372 31 (int.)
Fax (02) 8372 3809 (nat.), (+358-2-) 8372 3809 (int.)

Working Report 2020-01

Modelling Solute Transport and Water-Rock Interactions in Discrete Fracture Networks

David Applegate, Pete Appleyard, Steven Joyce
Wood

This work has been co-funded by Posiva and SKB

June 2020

MODELLING SOLUTE TRANSPORT AND WATER-ROCK INTERACTIONS IN DISCRETE FRACTURE NETWORKS

ABSTRACT

The radioactive waste disposal facilities at Olkiluoto in Finland and at Forsmark in Sweden, will be located in higher strength crystalline rock, where the groundwater is largely constrained to flow through sparse fracture networks. The chemical composition of the groundwater will play a key role in determining the safety of these geological disposal facilities, particularly the chemical stability of the buffer material and the resilience of the waste canisters. Chemical factors that are relevant for safety assessments include salinity, redox potential, pH and the concentration of a number of key chemical components.

In the past, safety assessments have followed one of two approaches to assess the hydrogeochemistry within fractured rock: (i) using an equivalent continuous porous media representation of the fracture network to model the transport and chemical interactions; or (ii) calculating steady state pressure solutions utilising explicit discrete fracture network models, then inferring the transport properties of the fracture network utilising particle tracking information. This report presents a new methodology, where the hydrogeochemical evolution is modelled using an explicit fractured rock representation. This has been accomplished by extending the discrete fracture network facility for the ConnectFlow groundwater flow and transport software to: (i) model solute diffusion into the pore space of the surrounding rock (i.e. matrix diffusion); (ii) solve the advection-diffusion equation for multiple solute species rather than just a single species (which is fully coupled to the pressure solution via the buoyancy term in Darcy's equation); and (iii) calculate chemical reactions of the groundwater solutes, possibly involving fracture/pore surface minerals or rock minerals, utilising an interface to the iPhreeqc library. Software parallelisation has significantly improved the performance of the code and extended the size of problems that can be solved.

The explicit representation of reactive transport within discrete fracture network models is a significant advance that allows groundwater flow, transport and hydrogeochemical reactions to be properly represented in a fractured bedrock. Preliminary hydrogeochemical calculations are presented for the ONKALO disposal facility at Olkiluoto, and the proposed Swedish repository for long-lived waste, SFL. These calculations show that DFN similations provide qualitatively similar results to those obtained from an ECPM representation. The ECPM is a more indirect approach, however, and differences do exist between the results from the DFN and the ECPM representations. These differences typically reduce as the resolution of the ECPM grid is increased.

Keywords: crystalline rock, discrete fracture network, geological disposal, safety assessment, matrix diffusion, reactive transport.

RAPORTTI KULKEUTUMISEN JA VESI-KALLIO-VUOROVAIKUTUKSEN MALLINNUS RAKOVERKOSSA

TIIVISTELMÄ

Ydinjätteen loppusijoituslaitokset Olkiluodossa Suomessa ja Forsmarkissa Ruotsissa rakennetaan kiteiseen kallioperään, jossa pohjaveden virtaus keskittyy toisiinsa kytkeytyneiden kalliorakojen harvaan verkostoon. Kalliopohjaveden kemiallinen koostumus on keskeinen tekijä loppusijoituslaitosten pitkäaikaisturvallisuuden, erityisesti puskurimateriaalien ja kapseleiden kestävyyden kannalta. Turvallisuusarviossa tärkeimpiä kemiallisia tekijöitä ovat pohjaveden suolapitoisuus, redox-potentiaali, pH ja eri kemiallisten yhdisteiden pitoisuudet.

Aiemmin turvallisuusarvioissa hydrogeokemian ja virtauksen vuorovaikutuksen mallinnus on perustunut joko ekvivalentin jatkuvan väliaineen malliin (ECPM) tai rakoverkkomallin avulla kuvattuun tasapainotilan vedenpaineeseen – jossa ei ole otettu huomioon veden tiheysvaihteluja – ja sen perusteella tuotettuihin tietoihin kulkeutumisominaisuuksista, ja virtausreiteistä. Tässä raportissa esitetään uusi menetelmä, jossa hydrogeokemian kehitys tuotetaan suoraan DFN-mallissa. Tämän toteuttamiseksi rakoverkkomalliin sisällytetään (i) virtauksen ja kulkeutumisen vuorovaikutus, joka aiheutuu diffuusiosta rakoa ympäröivän kiven huokosiin; (ii) advektio-diffuusio-yhtälön ratkaiseminen useammalle kuin yhdelle spesiekselle (jotka kytkeytyvät suoraan pohjaveden virtaukseen Darcyn yhtälön nostetermin kautta); (iii) kemiallisten reaktioiden, joissa otetaan huomioon rakojen ja huokoisrakenteen mineraalinen vaikutus, laskenta käyttäen iPhreeqc-aliohjelmakirjastoa. Ohjelmiston rinnakkaistaminen on parantanut sen suorituskykyä merkittävästi ja siten mahdollistanut suurempien mallinnusongelmien käsittelyn.

Reaktiivisen kulkeutumisen käsittely rakoverkkomallissa on merkittävä edistysaskel, joka mahdollistaa pohjaveden virtauksen, kulkeutumisen ja vesikemian reaktioiden keskinäisen kytkeytymisen rikkonaisen kallion yhdenmukaisessa esityksessä. Tässä raportissa alustavat hydrogeokemian laskut esitetään Olkiluodon ja Forsmarkin loppusijoituspaikoille. Rakoverkkomallin tulokset vastaavat kvalitatiivisesti ECPM:n tuloksia. ECPM on toisaalta epäsuorempi lähestymistapa, ja tulosten välillä on eroja. Erot tyypillisesti pienenevät, kun ECPM-laskentaverkko tihennetään.

Avainsanat: kiteinen kallio, rakoverkko, geologinen loppusijoitus, turvallisuusarvio, matriisidiffuusio, reaktiivinen kulkeutuminen

TABLE OF CONTENTS

1 INTRODUCTION

The chemical composition of groundwater plays an important part in determining the safety of geological radioactive waste disposal facilities (SKB 2011a, Salas et al. 2010, Trinchero et al. 2014). In particular, the hydrogeochemical evolution of the groundwater is one of the factors affecting the chemical stability of the buffer and resilience of the canisters. The factors relevant for a safety assessment include salinity, redox potential, pH and the composition of a number of key chemical components (SKB 2011a).

This report considers how the processes affecting hydrogeochemical evolution within a fractured rock can be modelled explicitly, accounting for some of the geometrical and hydrogeological properties of such environments. While the methods developed here are applied to the spent nuclear fuel repository at Olkiluoto and the proposed SFL facility in Sweden, they will also be relevant to other facilities hosted in fractured rocks.

1.1 Background

Understanding of the past hydrogeochemical situation at Olkiluoto (palaeo-hydrogeology), involves an integration of the hydrogeological description, climate re-construction, interpretation of groundwater samples (pore-water) from the rock mass and fracture mineralogy. The next subsection provides a summary. A more detailed discussion can be found in the comprehensive review on the subject by Smellie et al. (2014).

1.1.1 Hydrogeological description of Olkiluoto Island

Olkiluoto Island is roughly 12 km^2 in extent and is surrounded by shallow brackish seawater. It is topographically fairly flat with most areas less than 10 metres above the average sea level. Irregularities in the bedrock top surface are largely filled by a layer of Quaternary deposits, typically 2–5 metres in thickness.

The surface topography causes groundwater to flow down through the Olkiluoto bedrock. The flows are confined to a network of connected fractures that has arisen from various regional tectonic events that occurred during the Precambrian period. Hartley et al. (2012a) analysed drill-hole fracture data to ascertain an empirical relation between depth and the intensity and transmissivity of fractures in the Olkiluoto bedrock. This relationship subdivides recorded fractures into four depth zones, broadly as follows:

- Depth Zone 1 (DZ1): 0 to −50 m elevation; P_{10} intensity of all fractures 1.6 m^{-1}, P_{10} of water conducting fractures > 0.45 m^{-1}, Cl<1000 mg/L, Alkalinity > 150 mg/L, SO_4 < 250 mg/L;
- Depth Zone 2 (DZ2): −50 m to −150 m elevation; P_{10} intensity of 0.35 m^{-1}, P_{10} of water conducting fractures 0.15 to 0.45 m^{-1}, Cl>1000 mg/L, Alkalinity > 150 mg/L, SO_4 > 250 mg/L;
- Depth Zone 3 (DZ3): −150 m to −400 m elevation; P_{10} intensity of 0.35 m^{-1}, P_{10} of water conducting fractures 0.045 to 0.15 m^{-1}, 1000 < Cl < 4000 mg/L, 50<Alkalinity < 150 mg/L, SO_4 > 250 mg/L;

- Depth Zone 4 (DZ4): below −400 m elevation; P_{10} intensity of 0.19 m^{-1}, P_{10} of water conducting fractures < 0.045 m^{-1}, Cl > 4000 mg/L, Alkalinity < 50 mg/L, SO_4 < 250 mg/L.

Smellie et al. (2014) note that the groundwater salinities at Olkiluoto have a strong dependence on depth. Recent meteoric fresh water is found close to the surface; Littorina Sea water, together with glacial melt-water, exist between −200 to −300 m elevation; at greater depths increasingly saline groundwaters exist. Observations suggest that at very deep elevations (below −900 m elevation) salinities surpass 100 g/L (i.e. brines). The origin of the salinity is possibly from an evaporitic basin. The high density of the brines means the groundwater is almost immobile at depth.

Despite the large climatic variations during the Quaternary period, the infiltration of aerobic water has been systematically limited to few metres depth in the low transmissivity bedrock at Olkiluoto. Smellie et al. (2014) also note the existence of a distinct change in groundwater chemistry at −300 m elevation which is supported by a significant reduction in the intensity and transmissivity of connected fractures. These observations indicate that, at depth, the groundwater chemistry has been stable over a significant period during the Quaternary period (i.e. over several glacial cycles).

1.1.2 Hydrogeochemical evolution and its potential impact

Hydrogeochemical conditions at the Olkiluoto site will have a significant impact on the performance of the repository. The sorption of contaminents within the nearfield and geosphere is dependent on the chemical composition of the groundwater, particularly its pH. The stability of the bentonite buffer and the corrosion rate of the copper canister will also be affected by the composition of the groundwater.

The groundwater composition will evolve over time, driven by a combination of processes. Some of these will be due to construction of the repository itself while others will be naturally occurring processes.

1.1.2.1 Saline Upconing

Short-term hydrogeological impacts are expected during the repository construction and operation. The open tunnels and shafts of the ONKALO test facility, and the subsequent repository, will provide hydrogeological sinks to the site's groundwater system for about one hundred years. This may cause the drawing up of saline water from the deeper bedrock (saline upconing). Highly saline water is a concern for the performance of the tunnel backfill and buffer material, although the engineered barrier system has significant buffering capacity to counter this.

Previous calculations by Löfman & Karvonen (2012) considered the effects of saline upconing based on a continuous porous medium (CPM) model with homogeneous hydraulic conductivities within a few defined depth ranges and with uniform transmissivities within each hydrogeological zone. This provided an indication of the changes in salinity caused by construction of the disposal facility and how this was influenced by the fracture zones. Hartley et al. (2012b) also estimated the effect of saline upconing at Olkiluoto using both DFN and equivalent continuous porous medium (ECPM) models of a few deposition tunnels (described further in Section 2).

1.1.2.2 Grouting

Additional short term impacts include construction activities such as grouting and construction of cement repository strucutres. On the one hand, these can introduce further chemical constituents and alkalinity that can be transported and impact on repository safety functions. On the other hand, specific grouting activities, before the closure of the ONKALO, aim to reduce inflows to tunnels and deposition holes. This has been largely successful.

1.1.2.3 Longer term evolution

Current estimates (Posiva 2012a) suggest the current Holocene period will persist for the next 50,000 years (assuming anthropogenic climate change does not delay the onset of the next glacial period). During this period, the slow penetration of meteoric water into the bedrock could affect the performance of the bentonite buffer to some degree.

Hoek et al. (2016a) utilised both an analytical model and a transient multi-component solute transport calculation, using an ECPM representation, to quantify the possible future evolution of groundwater salinity in the bedrock surrounding the repository. A specified target was that the total charge equivalent of cations should stay above 4 mM to prohibit chemical erosion of the buffer. The analysis determined how many KBS-3H super containers (each super container consists of a canister surrounded by bentonite clay buffer and a perforated titanium shell) failed to meet this target. The main finding was that 5% to 15% of super containers experience cation concentrations below 4 mM. The lower bound estimate was determined from the ECPM calculations and the upper bound was determined from the analytic calculations.

Further hydrogeological impacts will result from the major climatic changes expected to occur during the next full glacial cycle. This cycle is expected to consist of several sequential periods of temperate, permafrost and glacial climate conditions. The different climate conditions affect the groundwater flow deep in the bedrock, which in turn may affect the performance of the disposal facilities.

CPM calculations by Löfman & Karvonen (2012) model the impact of these different climatic conditions. They note that the development of the permafrost decreases the hydraulic conductivity and infiltration into the bedrock, which affect the flow conditions during the permafrost periods. Consequently, the permafrost can interrupt the meteoric dilution experienced during temperate periods. Salinity levels during the permafrost periods are therefore largely constant.

During glaciation, the pressure of the overlying ice sheet is the major driving force to groundwater flow. The presence of the ice sheet determines the hydraulic gradients, which evolve with time as the ice margin moves across the site. Löfman & Karvonen (2012) have found that the location of the ice margin significantly affects the flow rates and directions in the repository rock volume. The flow rates follow the ice sheet evolution and are higher when the ice margin is above the site compared to the temperate and permafrost periods. However, when the ice sheet fully covers the site, the hydraulic gradients are significantly reduced. The changes to the salinity of groundwater in the repository host rock, resulting from the infiltration of glacial melt waters, are most significant when the ice margin is retreating over the repository area, in particular if the ice sheet stops at the site for hundreds or thousands of years.

1.1.3 Hydrogeochemical modelling with ConnectFlow

Wood developed a capability within ConnectFlow (Wood, 2018) to couple groundwater flow and solute transport with geochemical calculations (Joyce et al. 2014a, Joyce et al. 2014b) within ECPM/CPM. The geochemical calculations are carried out via an interface with the public domain iPhreeqc library (Charlton and Parkhurst 2011), which provides access to the capabilities of the widely used PHREEQC software (Parkhurst and Appelo 1999). A number of chemical reaction types have been developed so far, including equilibration with minerals, ion exchange, surface complexation and kinetic reactions. Reactions occurring within the rock matrix have also been included.

The reactive transport facility within ConnectFlow has been used to model the regional-scale evolution of groundwater composition at Forsmark involving different chemical reactions during an extended temperate climate period up to 60,000 AD (Joyce et al. 2014a, Joyce et al. 2014b). This was to address concerns by the Swedish regulator, SSM, regarding the implications for groundwater dilution and redox conditions within the repository volume during a prolonged period of meteoric water infiltration. Similar calculations were carried out for a spent nuclear fuel repository at Olkiluoto, illustrated for the KBS-3H concept, as part of a joint Posiva/SKB project (Hoek et al. 2016b).

1.1.4 Hydrogeochemical modelling within an explict DFN

The ECPM reactive transport models described above have provided some understanding of the potential evolution of groundwater composition on a large scale. However, these models do not properly capture the structural control on flow and transport processes imposed by a fracture network. This is because the upscaling process can give rise to unphysical connectivity between transmissive regions. Estimates of the kinematic porosity and flow-wetted surface of a fracture network may also be biased by the effect of fracture dead-ends.

Treating fractures in the context of a 3D discrete fracture network (DFN) allows a more realistic representation of the relevant transport and reactive processes than the single fracture treatments used in some reactive transport studies (e.g. Sidborn et al. 2014), which do not account for the discontinuous nature of the fracture system and the channeling of flow within them. Hartley et al, (2012b) presented a new approach to simulating the effects of underground openings on salinity directly within a DFN model. This was developed to illustrate some of the characteristics of saline upconing in a more representative discrete and heterogeneous groundwater system, and quantify some of the uncertainties affecting such simulations.

These DFN simulations of saline upconing induced by single tunnels do suggest that salinity changes are greatest around hydrogeological zones or large stochastic fractures, especially where they are sub-vertical and two such structures intersect one another. The simulation also showed that the influx of freshwater drawn down from the near-surface always acted to dilute the saline water upconing from below, creating a narrow transition zone around the open deposition tunnel, resulting in salinities of inflowing groundwater at the floor of the tunnel rarely above 35 g/L. Based on these limited simulations it was expected that there was one inflow point with salinity above 35 g/L per 3 deposition tunnels. The patterns of salinity were found to be reasonably consistent with those from ECPM models; provided sufficient refinement was used for the upscaling.

These DFN calculations were performed under steady-state conditions and did not include the effect of diffusion into the pore space of the rock (known as rock matrix diffusion or RMD). They also neglected chemical reactions involving solutes and mineral deposits on the fracture surfaces. ECPM calculations including all of these processes are becoming routine but so far have not been compared with explicit DFN calcuations. It is therefore uncertain how the well the ECPM approximation performs under these circumstances.

1.2 Objectives

This report describes a new approach to multi-component solute transport calculations, including rock matrix diffusion and hydrogeochemical reactions, in explicit structural models (i.e. DFNs). This method will allow the models to properly capture the characteristics of groundwater flow, solute transport, rock matrix interactions and chemical reactions within fractured crystalline bedrock. The approach is verified for single fracture models and simple fracture network models by comparison to ECPM equivalents. Applications are demonstrated for site-scale fracture networks at Olkiluoto and SFL.

This report is structured as follows:

- A baseline variable-density salt transport model for the Olkiluoto site is presented in Chapter 2, using both DFN and ECPM representations.
- In Chapter 3 a DFN implementation of rock matrix diffusion is described, and then applied to the Olkiluoto site-scale model from Chapter 2.
- The modelling of multiple reference waters within a DFN is addressed in Chapter 4 and the Olkiluoto site-scale models are updated to use this new algorithm.
- A DFN reactive transport implementation is described in Chapter 5. This is applied to a simplified model of SFL.
- Chapter 6 describes performance improvements that have been implemented in ConnectFlow (specifically parallelisation within DFN calculations). The new algorithms are used to simulate more detailed variants of the Olkiluoto site-scale model.

2 METEORIC WATER FLUSHING AT THE OLKILUOTO REPOSITORY

This chapter describes a baseline site-scale discrete fracture network (DFN) model of the Olkiluoto repository. This model has been developed to test variable density solute transport calculations representing the potential ingress of meteoric groundwater into the repository volume. A corresponding representation in an equivalent continuous porous medium (ECPM) model is also presented. Variations of this model will be used in later chapters to test the implementation physical processes such as rock matrix diffusion and multi-component solute transport.

2.1 Meteoric flushing of repository groundwater

The report by Hoek et al. (2016a) considers the possible future evolution of groundwater salinity in the bedrock surrounding the Olkiluoto spent nuclear fuel repository. A motivation for that work was the possibility that dilute groundwater could reach repository depth, which could adversely affect the bentonite buffer in the deposition drifts. A possible mechanism by which this may occur is meteoric water recharge under the temperate conditions that are assumed to persist until about 50,000 AD. Meteoric water may gradually displace and mix with the current saline water found at repository depth. The recharge occurs mainly at the relatively high ground in the centre of the Olkiluoto island, with downward vertical flow through the repository volume and then laterally to bays southwest and north of the site, but also with significant lateral dispersion of groundwater flow-paths to the east and southeast.

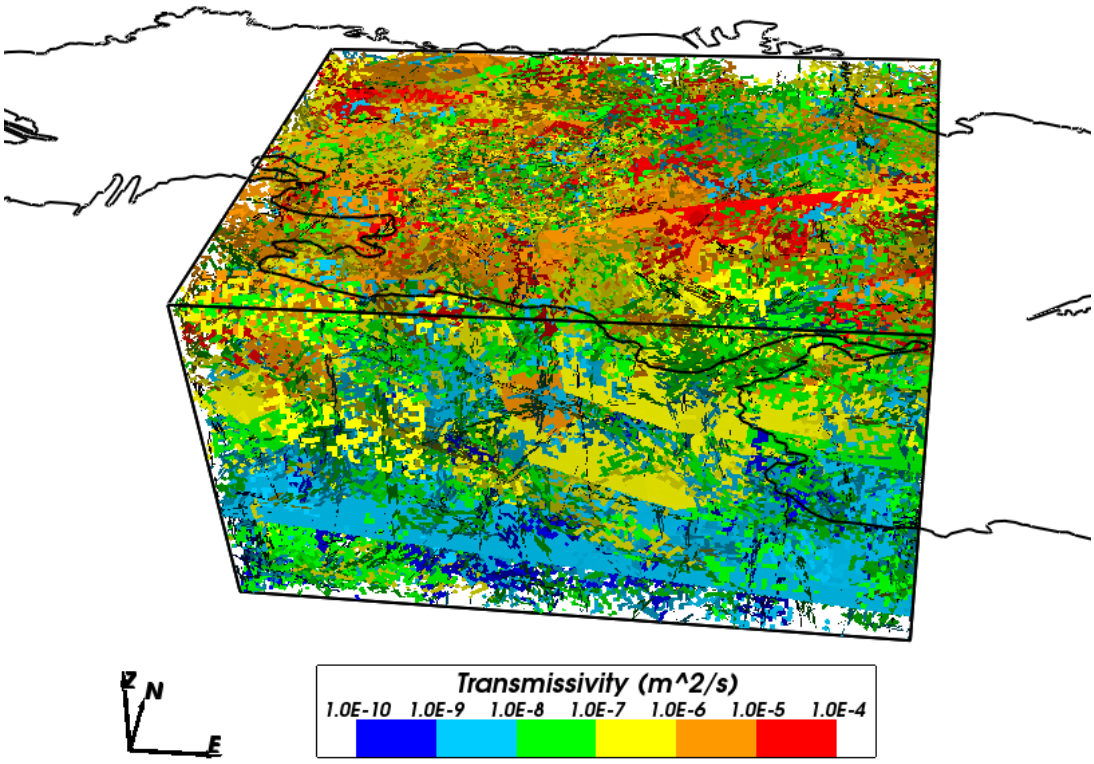

***Figure 2-1**. Site-scale DFN model for Olkiluoto. Fractures are coloured by transmissivity and the island outline is shown in black for context.*

Hoek et al. (2016a) utilise a nonlinear flux boundary condition to represent the top surface. For points above sea level, an infiltration is applied that automatically reduces at points where the head is just below the elevation (discharge occurs where the head exceeds the elevation). The boundary condition is modified for points beneath the sea. Infiltration occurs at points where the head is less than the hydrostatic pressure on the sea bed; discharge occurs at points where the head is greater than the hydrostatic pressure on the sea bed. Where recharge occurs, the infiltrating water is constrained to have sea water composition below sea level or have meteoric water composition above sea level. Where discharge occurs, there is no constraint on the composition of the water.

Circulation of groundwater to depth is limited because of the rapid reduction in fracture transmissivity with depth by about 3 orders of magnitude between the near-surface and repository depth, and to a lesser extent, the dominance of sub-horizontal fracturing, so that hydraulic gradients reduce with depth. The retardation of solute mixing fronts is thought to be compounded by a connected network of low transmissivity fractures that provides additional surface area for diffusive exchange with the rock matrix. This retardation process is crudely estimated for the calculations presented in this chapter but is explicitly modelled in the equivalent calculations presented in the next chapter.

Hoek et al. (2016a) utilised an analytical model and an ECPM transient multi-component solute transport calculation to quantify the possible evolution of groundwater salinity in the bedrock surrounding the repository. In the next section an explicit DFN model is developed to represent the same processes.

2.2 Model description

A site-scale model of Olkiluoto has been developed, which is 2.7 km by 2.1 km and is 1.4 km deep. The repository is centred at an elevation of –410 m. The top surface of the model is mapped to the surface topology at Olkiluoto. The model includes smaller fractures (above 20 m side length) around the repository. Larger fractures (above 200 m side length) and more intensly fractured, hydrogeologically active, deformation zones (hydrogeological zones) extend to the lateral boundaries (Figure 2-1). The model parameterisation is taken from the Olkiluoto Case C DFN model from SDM 2011 (Posiva 2011) and TURVA-2012 (Posiva 2012b) to produce a model that represents discontinuities and channelling within fracture planes. There are around 30,000 fractures in total (460,000 fracture tessellates).

A summary of the fracture statistics is given in Table 2-1. In this baseline model, the effects of rock matrix diffusion are represented using an effective transport aperture (fracture aperture plus immediate matrix pore volume). The simulations involve the flushing of saline groundwater by dilute meteoric water over two thousand years of the temperate period, i.e. it simulates the mixing of two waters. Calculations using this model are transient and represent the process of variable-density flow, advection, diffusion and dispersion within the fracture volume.

Table 2-1. *Fracture statistics for DFN.*

Property	Value	Units
Number of fractures	29,012	
Number of fracture tessellates	461,687	
Total P_{32}	$2.02 \cdot 10^{-2}$	m^{-1}
Hydrozone P_{32}	$2.56 \cdot 10^{-3}$	m^{-1}
Tessellation length	20	m

Table 2-2. *Summary of boundary conditions used in the DFN model. No flow boundary conditions are used, as an approximation, on the sides of the model. The physical system is expected to have some flow at these locations.*

Surface	Pressure	Concentration
Top	Initial value	Initial value
Sides	No flow	Initial value
Bottom	No flow	Initial value

2.3 Explicit DFN representation

2.3.1 Boundary conditions and initial conditions

The boundary conditions applied to the DFN model are summarised in Table 2-2. The initial value boundary conditions fix boundary pressures and concentrations equal to the initial condition throughout the duration of the simulation. The calculations represent the natural evolution of salinity and do not consider the impact of the repository itself. Therefore no boundary condition is required to represent pumping during the construction and operation of the repository.

The initial state of the model is interpolated from the results of a transient regional-scale ECPM simulation of the Olkiluoto site at 2000 AD (Posiva 2015). At this time, the distribution of salinity generally increases from the top of the model to the bottom and there is a low concentration of meteoric water at the depth of the repository. Due to the head gradient associated with the elevation of the Olkiluoto Island, the salinity distribution is expected to evolve with more meteoric water penetrating towards the repository. This will displace more saline water which will move laterally and then upwards beneath the sea.

The following procedure is used to convert between the results of the regional-scale model and the initial conditions for the smaller site-scale model.The groundwater density from the regional-scale model is interpolated onto the site-scale DFN. A steady-state flow calculation is then undertaken to determine a consistent pressure field. The pressure and

density from this calculation are then exported and used as an initial condition for the solute transport calculation. (The groundwater density ρ is converted to a saline concentration c using $c = \frac{\rho_B}{\rho}\frac{(\rho_F-\rho)}{\rho_F-\rho_B}$, where ρ_B is the density of brine and ρ_B is the density of freshwater).

Figure 2-2 shows the initial density distribution used for the DFN calculations. The density has been interpolated from the solution exported from the regional-scale ECPM model.

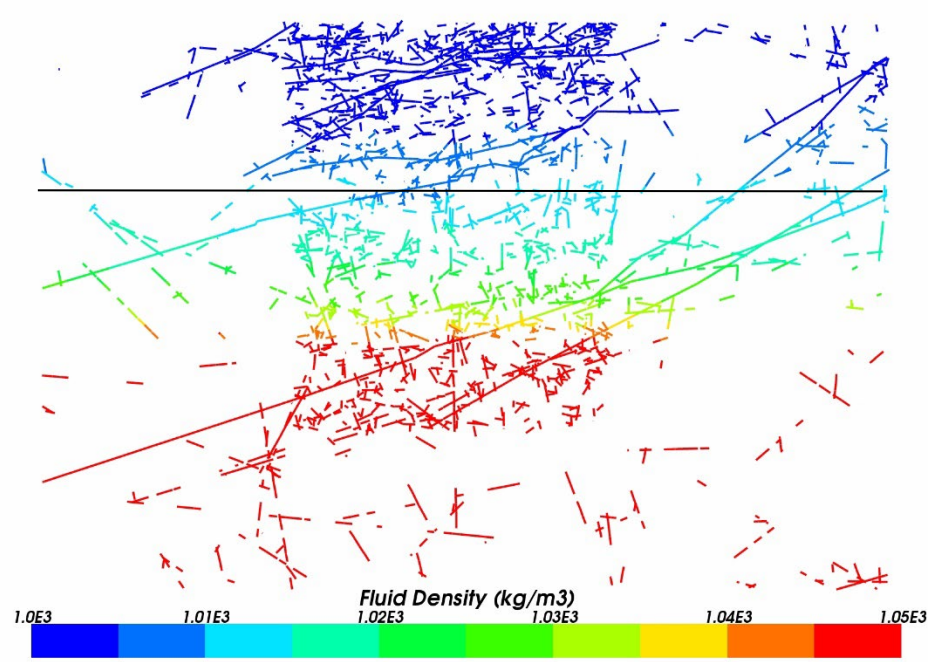

Figure 2-2. *Initial condition for groundwater density in the DFN. This slice through the model runs from the South on the left to the North on the right. It is centred at (1526000.0m, 6792100.0m). The black line represents the repository elevation at approximately −410 m. Note that smaller fractures (length less than 20m) are only included around the repository since this is where the concentration variation is of most interest. This does not reflect an increase in permeability around the repository.*

2.3.2 Transport properties

Solute transport within the DFN has been modelled in ConnectFlow as a fully coupled calculation of pressure and salinity (i.e. pressure affects the flow field and salinity distribution, which determines the density that feeds back to the pressure field through buoyancy). The salinity is effectively represented using two reference waters:

- Brine;
- Meteoric water (zero dissolved solids).

The density and viscosity of the two reference waters are given in Table 2-3. Summary of physical properties, together with the disperson/diffusion transport properties applied

within the fractured rock. The longitudinal dispersion length, at 20 m, is equal to the tessellation length of the fractures. The transverse dispersion length has a smaller size of 5 m.

Rock matrix diffusion (RMD) is included in the model which will be described in the next chapter. The RMD parameters used are given in Table 2-4. The initial condition for the salt concentration in the matrix is the same as the initial condition used for the fractures.

Table 2-3. *Summary of physical properties*

Property	Symbol	Value
Density of meteoric water	ρ_w	$9.9992 \cdot 10^2$ kg m^{-3}
Density of brine	ρ_b	$1.0514 \cdot 10^3$ kg m^{-3}
Viscosity	v	$1.0 \cdot 10^{-3}$ kg m^{-1} s^{-1}
Free solution diffusion coefficient	D_d	$1.0 \cdot 10^{-9}$ m^2 s^{-1}
Longitudinal dispersion length	a_L	20.0 m
Transverse dispersion length	a_T	5.0 m

Table 2-4*. RMD parameters for the site-scale case.*

Parameter	Symbol	Value
Matrix porosity	α	0.005
Intrinsic diffusion coefficient	D_i	$6 \cdot 10^{-14}$ m^2/s
Flow wetted surface (ECPM)	σ	3.238 m^2/m^3 (Depth Zone 1) 0.692 m^2/m^3 (Depth Zone 2) 0.698 m^2/m^3 (Depth Zone 3) 0.372 m^2/m^3 (Depth Zone 4)
Matrix diffusion length	w_{max}	$1/\sigma$ (Random fractures)
Number of RMD cells	n_{fv}	5
RMD cell lengths	w_i	$w_{max}/5$

2.4 Equivalent continuous porous medium (ECPM) representation

An equivalent ECPM model has also been created by upscaling the fracture network described above (this is distinct from the regional scale ECPM model used to interpolate the initial conditions). The upscaling calculates the equivalent permeability tensor and the kinematic porosity for a CPM mesh of 20 m finite elements filling the simulation domain. The upscaling process determines the equivalent permeability tensor for each finite

element using a number of calculations for unit head gradients applied between the different surfaces of the element. The resultant flows are used to compute the permeability tensor. The porosity is estimated from the proportion of void space due to connected fractures within an element, i.e. the sum of fracture surface area multiplied by transport aperture, divided by element volume. A full description of the method is provided in Hartley and Joyce (2013).

Unconnected fractures were removed from the DFN prior to the upscaling calculation to ensure the calculated values of porosity and permeability were not influenced by them. A guard zone was applied, meaning the bounding region of each upscaling cell was expanded to avoid edge effects. These edge effects can arise from isolated fractures directly connecting an inlet face to an adjacent outlet face, which can bias the effective hydraulic conductivity tensor towards high values.

The final upscaled mesh consists of nearly one million 20 m by 20 m by 20 m hexahedra. The permeabilities range from a specified minimum of 10^{-18} m^2 in elements containing no fractures (roughly 25% of elements have no fractures) up to 10^{-12} m^2 in elements containing high transmissivity fractures. The porosities range from 10^{-6} to ~10^{-4}. Table 2-5 summarises the properties of the upscaled finite element mesh.

Table 2-5. *Properties of the ECPM model.*

Property	**Value**
East-West extent	2.7 km
North-South extent	2.1 km
Vertical extent	1.38 km
Minimum permeability	10^{-18} m^2
Minimum porosity	10^{-6} m^2
Cell size	20 m, 20 m, 20 m

The transport properties used for the ECPM calculations are identical to those used for the DFN (See Table 2-3) except the transverse and longitudinal dispersion lengths are 50% larger, 7.5 m and 30 m respectively. Larger dispersion lentghs in the ECPM were employed, primarily, to reduce unphysical oscillations in the solution. However, the ECPM approximation will often provide a less tortuous route for transport than the original DFN, so it could be argued that a longer dispersion length may be appropriate in ECPM calculations.

Results for this model are presented in the final sections of the following two chapters.

3 ROCK MATRIX DIFFUSION IN A DFN MODEL

3.1 Background

Rock matrix diffusion (RMD) is a process whereby solutes diffuse between water flowing through fractures and less mobile water in the adjoining rock matrix under a concentration gradient (Neretnieks, 1980). This diffusion has the effect of retarding transport of solutes through the fractures. Because there may be a significant amount of pore surface area in the rock matrix, this is also a significant site for chemical reactions.

Two methods are included in ConnectFlow for calculating RMD in continuous porous media (CPM). The first is the analytic method introduced by Hoch and Jackson (2004), and the second is the finite volume method introduced by Joyce et al. (2014a). The analytic method is not appropriate for calculating chemical reactions, so the finite volume method is a more suitable method to implement in this context. This chapter describes the implementation of finite volume RMD for explicit DFN models.

The RMD implementation described here is appropriate for transport of a single solute. The implementation incorporated into ConnectFlow is a more general representation for multiple solutes (multi-solute transport is addressed in the next two chapters).

3.2 Mathematical representation of RMD in a DFN

The equations for the transport of saline water in a CPM affected by rock matrix diffusion (Joyce et al. 2014a, Hoch and Jackson 2004, and Carrera et al. 1998) are:

$$\frac{\partial\left(\phi_f \rho c\right)}{\partial t} + \nabla \cdot (\rho \vec{q} c) = \nabla \cdot \left(\phi_f \rho D \cdot \nabla c\right) + \sigma \rho D_i \left.\frac{\partial c'}{\partial w}\right|_{w=0}, \tag{3-1}$$

$$\alpha \frac{\partial (\rho c')}{\partial t} = \frac{\partial}{\partial w}\left(\rho D_i \frac{\partial c'}{\partial w}\right). \tag{3-2}$$

Here:

- ϕ_f (-) is equivalent porosity of mobile water in the fracture system or its porous media representation (but not including the porosity of the matrix).
- ρ (kg m^{-3}) is fluid density.
- c (-) is the concentration or fraction of saline water in the fracture.
- c' (-) is the concentration or fraction of saline water in the matrix.
- $\vec{q}$ (m s^{-1}) is Darcy flux in the fracture.
- t (s)is time.
- $D = \frac{D_d}{\tau}\delta_{lm} + a_T v \delta_{lm} + (a_L - a_T)\frac{v_l v_m}{v}$ (m^2 s^{-1}) is the dispersion tensor (including contribution from diffusion within the mobile water system of fractures or equivalent pores).
- τ (-) is the tortuosity.
- D_d (m^2 s^{-1}) is the free solution diffusion coefficient.
- D_i (m^2 s^{-1}) is the intrinsic diffusion coefficient for diffusion into the rock matrix, sometimes called the effective diffusion coefficient (this includes the capacity

factor and is therefore not equal to the free solution diffusion coefficient of the species).

- σ (m^{-1}) is the specific fracture surface area, i.e. the average fracture surface area per unit volume, sometimes called the flow-wetted surface area.
- w (m)is the distance into the matrix from the fracture surface.
- α (-) is the capacity factor, which is equivalent to the porosity of the matrix when there is no sorption in the rock matrix.

For a DFN model, the effective aperture of a fracture accessible to mobile water is characterised by the transport aperture, e_t, and the available volume for matrix diffusion is characterised by the length of the intervening matrix blocks between fractures, s_b. The equivalence relationships with the CPM parameters described above are:

$$\phi_f = \frac{e_t}{s_b + e_t} \cong \frac{e_t}{s_b} = \frac{e_t \sigma}{2}. \tag{3-3}$$

Substituting for ϕ_f and σ into Equation (3-1), and converting the Darcy flux vector, $\vec{q}$, to a flow per unit width, $\vec{Q} = 2\overrightarrow{q/\sigma}$ (i.e. transmissivity times head gradient vector), the transport equation for the DFN is obtained:

$$\frac{\partial(e_t \rho c)}{\partial t} + \nabla \cdot \left(\rho \vec{Q} c\right) = \nabla \cdot (e_t \rho D \cdot \nabla c) + 2\rho D_i \left.\frac{\partial c'}{\partial w}\right|_{w=0} \tag{3-4}$$

$$\alpha \frac{\partial(\rho c')}{\partial t} = \frac{\partial}{\partial w}\left(\rho D_i \frac{\partial c'}{\partial w}\right) \tag{3-5}$$

The penetration depth into the matrix is bounded to half the matrix block size ($w < s_b/2$). This is because the solute diffusion fronts typically propagate through a matrix block from both sides so that the effective penetration depth for each fracture is halved. Sudicky and Frind (1982) presented an analytic solution for RMD within an idealised two fracture system which is described in the next section.

3.2.1 Analytic solution for RMD within an idealised two fracture system

Figure 3-1 is a two dimensional representation of two identical parallel fractures, distance s_b apart, within a porous matrix. Fluid within the fractures moves vertically downwards from $z=0$ at a velocity v. Sudicky and Frind (1982) derived an analytic solution for solute transport within this system, given an equilibrium at $t=0$ with concentration C_0 (in both the fracture and the matrix) and a continuous injection of a fluid of concentration C_s at $z=0$. The initial and boundary conditions for equation (3-4) are then:

$$c(z,0) = C_0$$

$$c(0,t) = C_s$$

$$c(\infty,t) = C_0 \tag{3-6}$$

For the matrix diffusion equation (3-5) the initial and boundary conditions are:

$$c'(w,z,0) = C_0 \tag{3-7}$$

$$c'(0,z,t) = c(z,t) \tag{3-8}$$

$$\frac{\partial c'}{\partial w}\left(\frac{s_b}{2},z,t\right) = 0 \tag{3-9}$$

Assuming the effect of dispersion and diffusion within the fracture are minimal, Sudicky and Frind (1982) derived a transient solution for the RMD process. Ignoring sorption and radioactive decay, their solution is:

$$\frac{C_0 - c(z,t)}{C_0 - C_s} = \frac{2}{\pi}\int_0^\infty \frac{1}{\varepsilon}\exp\left(\varepsilon_R^0\right)\left(\sin\varepsilon_I^0 + \sin\Omega^0\right)d\varepsilon \tag{3-10}$$

for time $t > t_w = \frac{z}{v}$, (the advective travel time), and where,

$$\varepsilon_R^0 = -\frac{\omega\varepsilon}{2}\left(\frac{\sinh(\theta\varepsilon) - \sin(\theta\varepsilon)}{\cosh(\theta\varepsilon) + \cos(\theta\varepsilon)}\right), \tag{3-11}$$

$$\varepsilon_I^0 = \frac{\varepsilon^2(t - t_w)}{2} - \frac{\omega\varepsilon}{2}\left(\frac{\sinh(\theta\varepsilon) + \sin(\theta\varepsilon)}{\cosh(\theta\varepsilon) + \cos(\theta\varepsilon)}\right), \tag{3-12}$$

$$\Omega^0 = \frac{\omega\varepsilon}{2}\left(\frac{\sinh(\theta\varepsilon) + \sin(\theta\varepsilon)}{\cosh(\theta\varepsilon) + \cos(\theta\varepsilon)}\right), \tag{3-13}$$

$$\theta = \frac{\alpha^{1/2}}{2D_i^{1/2}}(s_b - e_t), \tag{3-14}$$

$$\omega = \frac{2(\alpha D_i)^{1/2} t_w}{e_t}. \tag{3-15}$$

Equation (3-10) is differentiable with respect to $t' = t - t_w$, resulting in the expression:

$$\frac{dc}{dt'} = \frac{C_s - C_0}{\pi}\int_0^\infty \varepsilon\exp\left(\varepsilon_R^0\right)\cos\varepsilon_I^0 d\varepsilon. \tag{3-16}$$

This can then be used in a Newton-Raphson iteration scheme toward the breakthrough time at which the concentration equals the target concentration C_T

$$t_T'' = t_T' - \frac{c - C_T}{\frac{dc}{dt'}} \tag{3-17}$$

This analytic result is used to verify numerical ConnectFlow calculations later in this chapter.

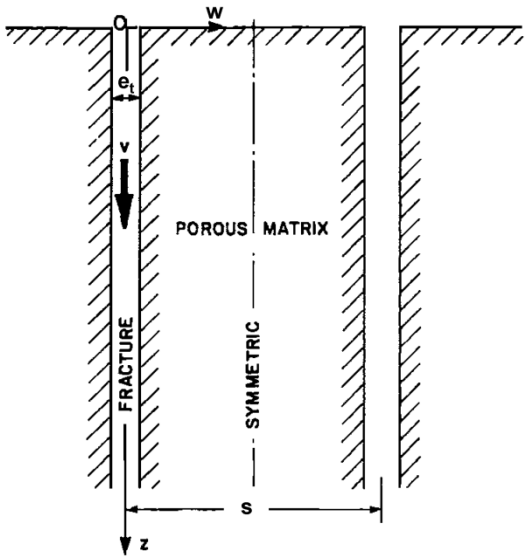

Figure 3-1. *Idealised fracture-matrix system of regularly spaced fractures (after Sudicky and Frind, 1982).*

3.3 Implementation of RMD in ConnectFlow

Joyce et al. (2014a) describe a numerical method for calculating the diffusive flux into the matrix of a CPM model (R_{CPM}). This method utilises a finite volume discretisation of the matrix. The discretisation of equation (3-1) then gives the following expression for the dffusive flux into the matrix,

$$R_{CPM} = \sigma\rho D_i \left.\frac{\partial c'}{\partial w}\right|_{w=0} = \frac{2\sigma\rho D_i}{\Delta w_1}\left(c'^{n+1}_1 - c^{n+1}\right), \tag{3-18}$$

where n defines the timestep. In this expression, the finite volume adjacent to the fracture has length Δw_1 and concentration c'^{n+1}_1. Importantly, the concentration adjacent to the fracture can be written in the form,

$$c'^{n+1}_1 = A' + c^{n+1}B', \tag{3-19}$$

where the factors A' and B' are calculated using matrix concentrations from the previous timestep. This simplifies the calculation of the matrix and fracture concentrations by significantly reducing the number of concentrations that have to be solved simultaneously.

The method employed for a DFN is identical, except for a factor of $\sigma/2$. Hence, for a DFN model, ConnectFlow reuses many of the algorithms that already exist for a CPM model. The most important differences in implementation arise from the fact that in a CPM model the equations are applied for each finite-element in the grid, while in a DFN model the equations are applied for each sub-fracture (also known as a tessellate). In ConnectFlow, fractures are composed of sub-fractures, which themselves are composed

of finite elements. Increasing the number of sub-fractures used to model a larger fracture or deformation zone provides greater spatial resolution for the transfer between fracture and matrix as a solute mixing front moves through the network.

The following new parameters have been introduced into the DFN in order to represent RMD:

- An instruction as to whether RMD is to be used or not;
- The total diffusion length into the matrix w_{max} or the length of each finite volume cell, w_i;
- The number of finite volume cells, n_{fv};
- The intrinsic diffusion coefficient, D_i;
- The matrix porosity, α.

It is important to note the distinction between the matrix block size, $s_{b,}$ and the maximum diffusion length into the matrix, w_{max}. The matrix block size is the distance to the next fracture. The diffusion length is the distance that is accessible for RMD, which is typically half the matrix block size since the adjacent fracture will affect the other half of the matrix block.

The parameters D_i, w_{max} and α can be defined on a fracture-by-fracture basis for deterministic fractures and by fracture set for stochastically-generated fractures. The number of finite volume cells is the same for *all* fractures in a model and their sizes are the same for every fracture in a set. This contrasts with CPM modelling where the equivalent parameters are defined by rock type.

Alternatively, the user can choose to not specify w_{max} and allow ConnectFlow to automatically calculate it. In this calculation, w_{max} is the smallest normal distance from the centre of a sub-fracture to another sub-fracture in the DFN. In one sense this calculation is crude since it does not consider the orientation or extent of the neighbouring sub-fracture. However, the approximation should improve as the number of sub-fractures within a fracture is increased.

However w_{max} is determined, (whether it is automatically calculated or specified by the user) the following consistency checks are made to ensure $\sum_{i=1}^{n_{fv}} w_i = w_{max}$:

- If $\sum_{i=1}^{n_{fv}} w_i < w_{max}$ then $w_{n_{fv}}$ (the last block) is increased to ensure the equality.
- If $\sum_{i=1}^{n_{fv}} w_i > w_{max}$ and w_{max} is chosen by the user (rather than automatically) then w_{max} is increased to ensure the equality.
- If $\sum_{i=1}^{n_{fv}} w_i > w_{max}$ and w_{max} is determined automatically then the number and/or length of the w_i are reduced to ensure the equality

In addition, it is necessary to be able to specify the initial concentration of solute in the matrix. It is possible that the initial condition, as specified, will be somewhat artificial and not consistent with a system that has evolved over a long period. Hence, there is an optional facility to equilibrate the initial solute concentrations between the fractures and matrix for a specified time before carrying out a solute transport calculation. This effectively runs the RMD calculation for a certain period to allow the matrix solute

concentration to reach equilibrium with the fractures before the beginning of the solute transport calculation, so that the initial state of the fractures and matrix is more consistent.

3.4 Verification

To verify RMD in a DFN, a series of tests were performed of increasing complexity. These compare the DFN results with those from equivalent CPM models and with values predicted by the analytic model Equation (3-17).

3.4.1 Single-fracture case

The first test is a simple cuboid block of rock extending from x=0 to x=10,000 metres with a 100 metre by 100 metre cross-section in the y and z directions. The block contains a single fracture spanning its entire length in the x and y directions. The model parameters for the block are given in Table 3-1. A DFN representation of this system has been constructed with the fracture subdivided into square tessellates of side length 100 metres. An equivalent two-dimensional CPM case has also been assembled where the block of rock is divided into 100 cubic finite elements, each with a side length of 100 metres.

Dirichlet boundary conditions are imposed at x=0 metres with a head of 50 metres and a saline mass fraction of 1.0. At x=10,000 metres, a head of 0 metres is imposed and an outflow boundary condition is applied for the solute. The initial saline mass fraction is set to zero throughout the block. Buoyancy effects have been removed by setting the density of the saline water equal to that of the freshwater.

In each case (CPM and DFN), the equations for solute transport are solved both with and without rock matrix diffusion in a transient simulation over a period of 10^{10} seconds. The density of the fluid is held fixed and the storativity of the rock is assumed to be zero. Five equal sized finite volume blocks have been used to calculate the RMD for both the CPM and DFN calculations.

Figure 3-2 shows the mass fractions at x = 5000 metres in each calculation. The effect of RMD is seen to produce a significant retardation in the rate of transport. The DFN and CPM results are in good agreement, both with and without the effect of RMD.

The figure also includes CPM results calculated using a semi-analytic approach (this is an alternative RMD algorithm in ConnectFlow and is distinct from the fully analytic model presented in Equation (3-16)). Both CPM and DFN finite volume RMD results are slightly different from the model calculated with semi-analytic RMD. This difference is due to the small number of equally-sized finite volumes. Joyce et al. (2014a) found that using smaller finite volumes closer to the fractures and larger finite volumes further away, improves the match between semi-analytic and finite volume cases. Note that, modifying the tessellation length did not affect the results.

Finally, several DFN calculations are performed with different values of diffusion length, matrix capacity and matrix diffusion coefficient. The retardation factors (retarded/unretarded travel time) from these calculations are extracted and compared with the values predicted by the fully analytic model presented in Equation (3-17) The results, presented in Table 3-2, reveal good agreement between the ConnectFlow calculations and the analytic expression for a variety of model parameters.

Table 3-1. *Parameters used for the single-fracture case. Note the saline and fresh water density have been set to the same value to remove buoyancy from the problem.*

Parameter	**Symbol**	**Value**
Salt diffusion coefficient	D_{salt}	10^{-9} m^2/s
Longitudinal dispersion length	$l_{D_{long}}$	100 m
Transverse dispersion length	$l_{D_{trans}}$	10 m
Effective porosity (CPM)	ϕ_f	0.02
Transport aperture (DFN)	e_t	0.02 m
Density of fresh water	ρ_{wat}	998.22 kg/m^3
Density of saline solution	ρ_{sol}	998.22 kg/m^3
Matrix porosity	α	0.3
Matrix diffusion coefficient	D_i	$5 \cdot 10^{-11}$ m^2/s
Fracture Area per unit Volume (CPM)	σ	2.0 m^2/m^3
Matrix diffusion length	w_{max}	0.49 m
Number of RMD cells	n_{fv}	5
RMD cell lengths	w_i	0.098 m
Storativity (DFN)	S_{DFN}	0
Specific storage coefficient (CPM)	S_{CPM}	0 m^{-1}

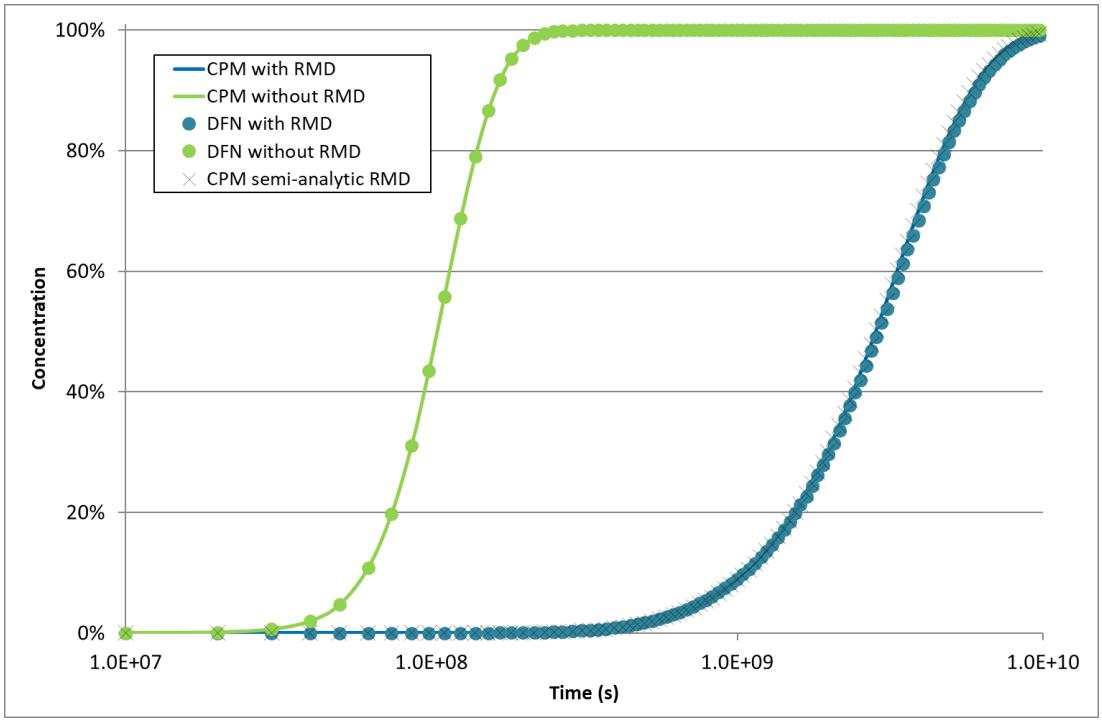

Figure 3-2. *Comparison between modelled mass fractions at x = 5000 metres (half way) down the block containing a single fracture. Solid lines mark the CPM data, circles mark the DFN data, and CPM semi-analytic RMD is included for comparison.*

Table 3-2. *Retardation factors for variants of the single fracture case. Three retardations are reported: ConnectFlow with 5 finite volumes, ConnectFlow with 500 finite volumes and a calculated value from solving Equation (3-16). Note that the 4th result shows the greatest difference between 5 and 500 finite volumes because the diffusion coefficient is smallest, resulting in the smallest penetration depth into the matrix. This requires a higher refinement to resolve.*

Matrix Capacity	**Matrix Diff. Coefficient (m^2/s)**	**Diffusion Length (m)**	**Retardation factor 5 Finite vols.**	**Retardation factor 500 Finite vols.**	**Retardation factor (Calculated)**
0.3	$5.0 \cdot 10^{-11}$	0.495	28.4	28.8	29.0
0.3	$2.0 \cdot 10^{-10}$	0.495	29.8	29.9	30.0
0.3	$1.0 \cdot 10^{-11}$	0.495	20.5	22.4	22.8
0.3	$3.0 \cdot 10^{-12}$	0.495	5.5	8.9	9.1
0.1	$5.0 \cdot 10^{-11}$	0.495	10.1	10.3	10.3
0.6	$5.0 \cdot 10^{-11}$	0.495	55.9	56.6	57.0
0.3	$5.0 \cdot 10^{-11}$	0.1	6.8	6.8	6.6
0.3	$5.0 \cdot 10^{-11}$	0.9	48.6	49.4	49.9

3.4.2 Two-fracture case

A two-fracture test case was simulated as shown in Figure 3-3. The two fractures are identical in size at 102.6 m long. One fracture intersects with the boundary on the left-hand side and the other intersects with the boundary on the right-hand side. The two fractures intersect half way between the left- and right-hand boundaries. There is a significant "dead end" on each fracture, which is a part of the fracture that is only connected at one end to another fracture or boundary. The fractures are modelled explicitly using a DFN approach with a tessellation length of 5 m.

Dirichlet boundary conditions are applied on the left-hand boundary with a head of 51.1 m and a saline concentration of 1.0. On the right-hand boundary, a head of 0 m is applied and an outflow condition is applied for the salinity. The total flow path from the left to the right is 106.4 m. The transport parameters used in this test case are listed in Table 3-3.

Solute transport calculations are carried out for this model, both with and without RMD. Additionally, a particle tracking calculation is performed to test the advective (non-RMD) transport properties of the system. Finally, a value for the RMD retardation is calculated using Equation (3-17).

Table 3-4 gives the results for these calculations. The particle tracking calculation and non-RMD transport calculation give good agreement for the travel times. The retardation indicated by the ConnectFlow RMD calculation is also in good agreement with the analytic value (the analytic RMD method was discussed in section 3.2.1).

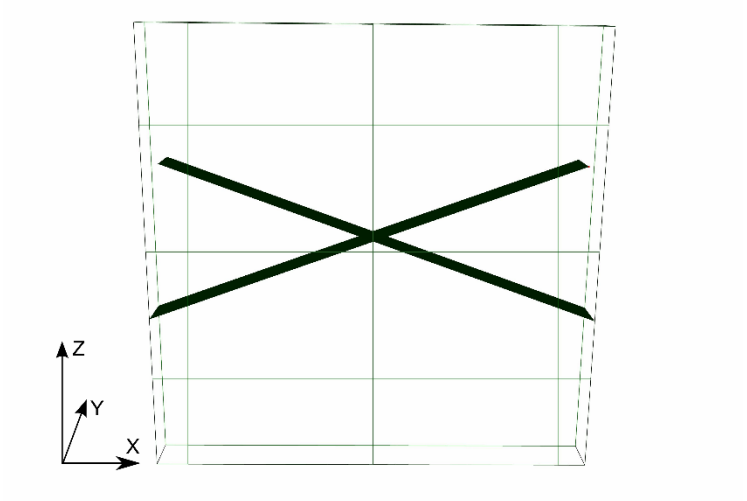

Figure 3-3. *Two fracture test case. Notice the two fractures only intersect the model boundary once each in the bottom half of the model.*

Table 3-3. *Parameters for two fracture test.*

Parameter	Symbol	Value
Salt diffusion coefficient	D_{salt}	10^{-14} m^2/s
Longitudinal dispersion length	$l_{D_{long}}$	5 m
Transverse dispersion length	$l_{D_{trans}}$	5 m
Transport aperture	e_t	0.0001 m
Transmissivity	T	$1.635 \cdot 10^{-7}$ m^2/s
Density of fresh water	ρ_{wat}	998.22 kg/m^3
Density of saline solution	ρ_{sol}	998.22 kg/m^3
Matrix porosity	α	0.0008
Matrix diffusion coefficient	D_i	$5 \cdot 10^{-10}$ m^2/s
Matrix diffusion length	w_{max}	1.0 m
Number of RMD cells	n_{fv}	5
Storativity	S_{DFN}	0

Table 3-4. *Results for two fracture test.*

Particle travel time	$1.34 \cdot 10^5$ s
No RMD transport time	$1.35 \cdot 10^5$ s
RMD transport time	$2.1 \cdot 10^6$ s
ConnectFlow finite volume retardation factor	15.6
Calculated retardation factor (analytic)	14.5

3.4.3 Stochastic DFN case

A more elaborate test considers a stochastically generated DFN. The model domain is a cuboid of length 500 metres along the x axis, from $x = 0$ metres, with a square cross-section of side length 50 metres. Instead of a single fracture, the block contains a stochastically-generated fracture network designed to allow flow across the block.

The model (illustrated in Figure 3-4) contains 891 square fractures, divided between two sets, each fracture sized between 10 metres and 35 metres in side length, generated using a triangular distribution (of mode 15 metres). Fractures dip gently along the axis of the block (one set dipping one way, the other set dipping the other way), to create connectivity between fractures. Fractures that do not contribute to steady-state flow (because they are isolated from the wider network or only connect to the network at a single intersection) are removed from the model before a solution is calculated.

Fracture transmissivity (T) in both sets is based on a log-normal distribution, such that mean $\ln(T) = -20.7$ (i.e. $T \approx 10^{-9}$) and the standard deviation of $\ln(T)$ is 2. The distribution was truncated at $\ln(T) = -25.3$ ($T \approx 10^{-11}$) and $\ln(T) = -16.1$ ($T \approx 10^{-7}$). Transmissivity in this model is not correlated with fracture size.

To allow comparison between this model and an ECPM, the fracture network is upscaled using a grid of 0.2-metre cells, creating an ECPM containing 156,250 finite elements. This is shown, with low-permeability finite elements excluded, in Figure 3-5.

As with the one-fracture case, a head of 50 metres and a mass fraction of 1.0 is set at $x = 0$, and zero head and zero mass fraction are set at the far end of the model ($x = 500$ metres in this case). The initial mass fraction is zero.

The model parameters for the block are given in Table 3-5.

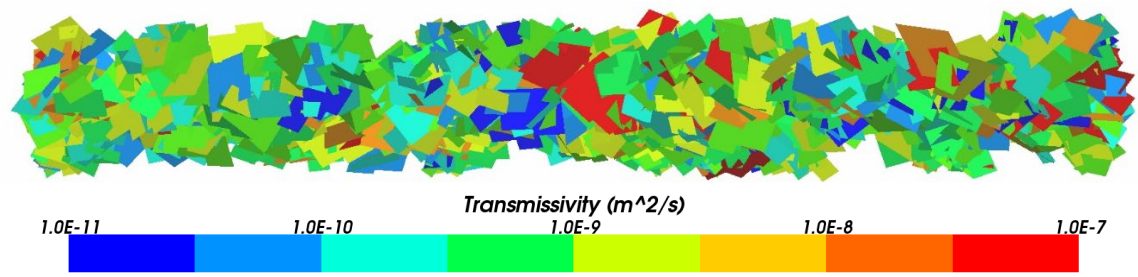

Figure 3-4. *Image of fractures in the simple stochastic fracture block, coloured by transmissivity.*

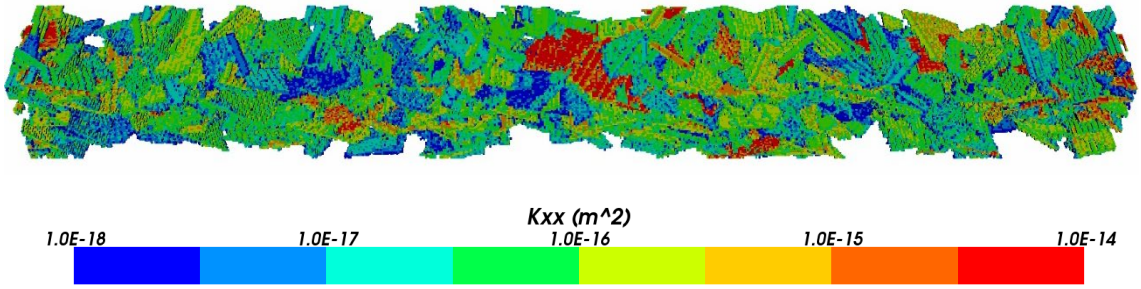

Figure 3-5*. Image of the equivalent CPM to the fractures shown in Figure 3-4 coloured by permeability. To allow greater clarity, finite elements whose permeability is less than 10^{-18} m^2 have been excluded from this visualisation.*

Table 3-5. *List of parameters for the stochastic block case.*

Parameter	Symbol	Value
Salt diffusion coefficient	D_{salt}	10^{-9} m^2/s
Longitudinal, transverse dispersion length	$l_{D_{long}}$, $l_{D_{trans}}$	7 m
Transverse dispersion length		1.4 m
Density of water	ρ_{wat}	998.22 kg/m^3
Density of saline solution	ρ_{sol}	998.22 kg/m^3
Matrix porosity	α	10^{-4}
Intrinsic diffusion coefficient	D_i	$5{\cdot}10^{-12}$ m^2/s
Fracture Area per unit Volume (CPM)	σ	0.481 m^2/m^3
Matrix diffusion length	w_{max}	2.08 m
Number of RMD cells	n_{fv}	5
Storativity (DFN)	S_{DFN}	0
Specific storage coefficient (CPM)	S_{CPM}	0 m^{-1}

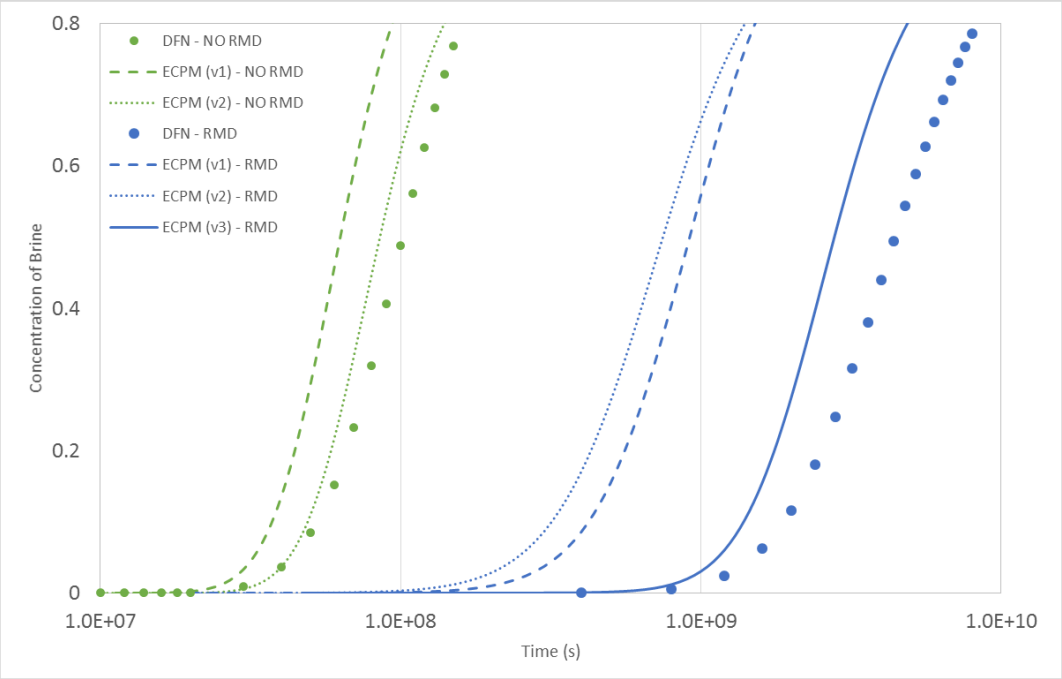

Figure 3-6. *Comparison between concentrations at x = 250 metres (half way) down the block of stochastic fractures, comparing DFN with ECPM and comparing with and without rock matrix diffusion (RMD). Multiple versions of the ECPM model are included in the figure. ECPM (v1) uses 0.2m finite elements. ECPM (v2) uses 0.083m finite elements. ECPM (v3) uses 0.083m finite elements and an upscaled flow wetted surface for each element rather than the average flow wetted surface for the model.*

A plot of mass fraction at the centre point over time is shown in Figure 3-6 for DFN and ECPM models, both with and without RMD. The ECPM model, as discussed above, is labelled ECPM (v1). The salinity in the DFN travels somewhat more slowly than in the ECPM (v1), without RMD. When RMD is included the results are even further apart and the transport speed in the DFN is a factor of four slower.

It is to be anticipated that the ECPM and DFN results in such a model will not be as closely matched as in the single-fracture case. By its nature, a continuum model may provide flow paths that do not exist in the actual DFN, due to instances where two fractures are close enough to share the same upscaled block but do not actually intersect. Additionally, the upscaled porosity does not consider the anisotropy of the fractures (presumably a "tensor" porosity would be needed for a better approximation). For this example, these effects are expected to be somewhat mitigated by the relative homogeneity of this DFN and the very small block size in the ECPM (substantially smaller than the mean matrix block size, meaning that the ECPM will frequently resolve to the level of individual fractures), but nonetheless, it is to be expected that the flow characteristics of the ECPM will be somewhat different to those in the DFN (given the current limitations of the upscaling calculations).

It should be possible to obtain a better match between the ECPM and DFN models by increasing the resolution of the upscaling. ECPM (v2) in Figure 3-6 has a much finer resolution than ECPM (v1) with a 0.083m finite element size. This is much closer to the DFN results when RMD is ignored, as expected, but is slightly worse when RMD is included. This peculiar result suggests there is something not quite right with the upscaling. Closer investigation revealed that the existing upscaling algorithm in ConnectFlow calculates the porosity and permeability, which is sufficient for non-RMD calculations, but does not approximate the flow wetted surface (σ in Equation 3.1). Instead the flow wetted surface is taken to be twice the fracture surface area per unit volume averaged over the entire model. This means the effective matrix diffusion area in the main volume through which the solute travels is significantly reduced by using an average from parts of the model that the solute does not (mainly) travel through. To address this, the flow wetted surface was also upscaled and a new calculation was run – ECPM (v3). The results of this calculation are much closer to the DFN RMD calculation. (Note that the updated upscaling algorithm is available in ConnectFlow 12.0, Wood, 2018).

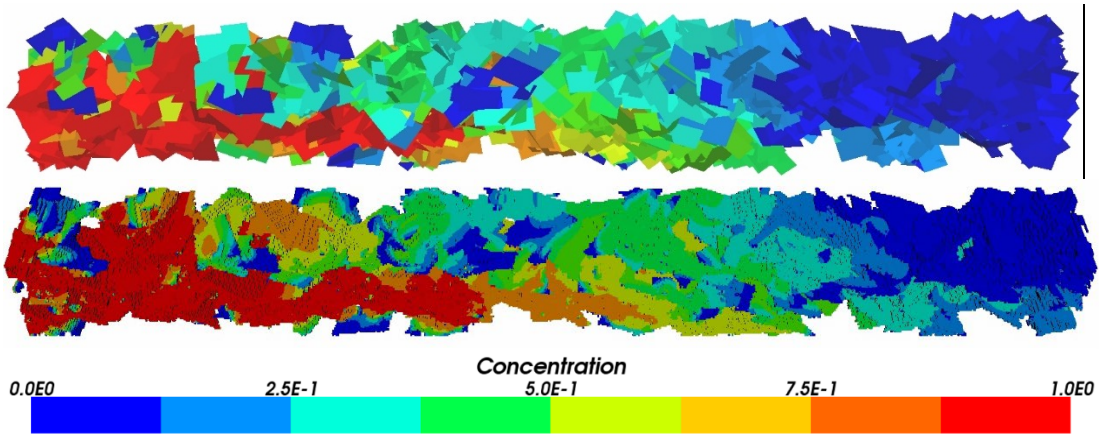

Figure 3-7. *Comparison of mass fractions in a stochastic DFN model without RMD (top) with an equivalent ECPM model (bottom) at time $1.6125 \cdot 10^8$ seconds. For clarity, finite elements whose permeability is less than 10^{-18} m^2, are hidden.*

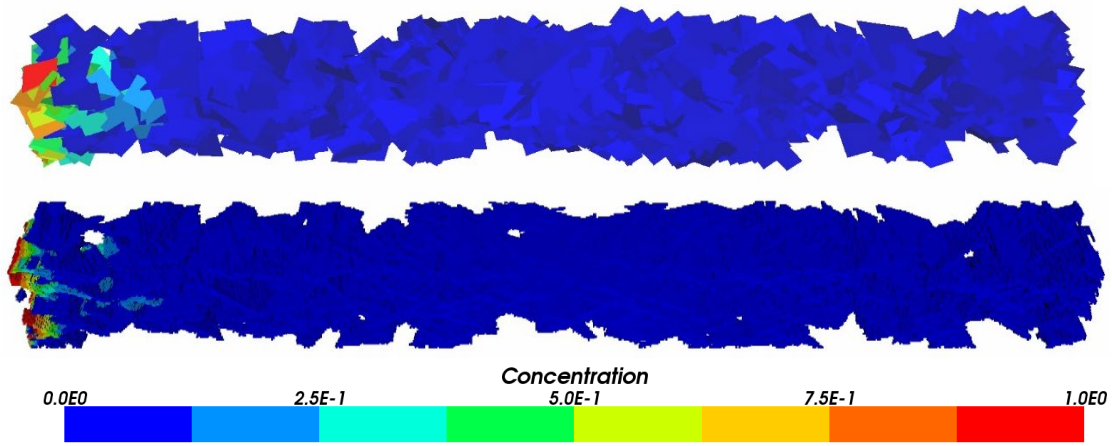

Figure 3-8. *Comparison of mass fractions in a stochastic DFN model with RMD (top) with an equivalent ECPM model (bottom) at time $1.6125 \cdot 10^8$ seconds. For clarity, finite elements whose permeability is less than 10^{-18} m^2, are hidden.*

Table 3-6 gives a summary of the results for the stochastic fracture case. The retardation of the DFN model is in excellent agreement with that suggested by analytic calculations. The best ECPM model (v3) is also in reasonable agreement but has a smaller retardation. The effect of RMD on salinity at a specific time is shown in Figure 3-7 and Figure 3-8 for DFN and for ECPM (v3) calculations.

Table 3-6. *Summary of results for random fracture case. The analytic retardation is calculated using equation (3-17).*

Result	**Value**
DFN travel time without RMD	$1.02 \cdot 10^8$ s
ECPM (v2) travel time without RMD	$8.55 \cdot 10^7$ s
DFN travel time with RMD	$4.08 \cdot 10^9$ s
ECPM (v3) travel time with RMD	$2.78 \cdot 10^9$ s
Retardation for ECPM (v3)	32.6
Retardation for DFN	40.1
Analytic Retardation	39.6

3.5 Olkiluoto Site Scale Model

The rock matrix diffusion implementation is included in a simulation of meteoric water intrusion at Olkiluoto. This model was presented in detail in Chapter 2. Results from the DFN and ECPM calculations are given in Figure 3-9. The downwards intrusion of dilute meteoric water in the centre of the model is clear in both the DFN and ECPM models. The more saline water at repository depth appears to be displaced towards the lateral boundaries of the model. The behaviour of the DFN and ECPM in this instance is very closely matched with only slight differences between them. The main differences are that the dilute water appears to penetrate less evenly and in more confined regions in the DFN model when compared with the ECPM model. This is probably due to unphysical additional connectivity inherent in the ECPM approximation, which allows a more even penetration of the dilute water.

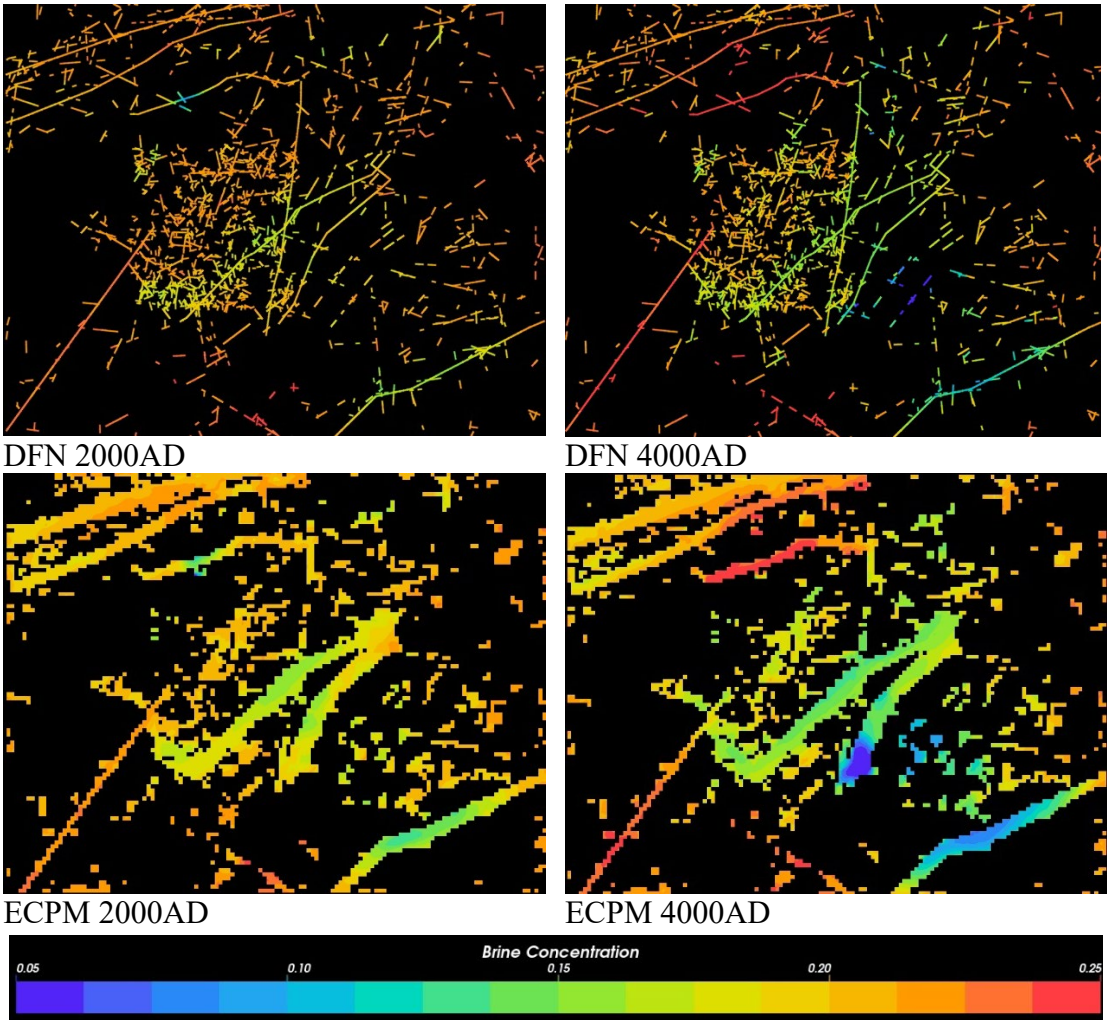

Figure 3-9. *Evolution of salinity over 2000 years at the Olkiluoto site. ECPM and DFN models are shown and both include RMD explicitly. These horizontal slices are at −400m depth.*

4 TRANSPORTING MULTIPLE SOLUTES

4.1 Background

Prior to the developments described in this report, the DFN functionality of ConnectFlow was limited to the transport of a single salt species (coupled with the pressure calculation via the density). This chapter describes how this functionality has been extended to include the simultaneous transport of multiple salt components, fully coupled with the pressure calculation. This brings the solute transport capabilities of the DFN in line with the existing CPM functionality of ConnectFlow. This facility allows the chemical composition of the groundwater to be explicitly modelled as a function of time which is highly relevant to the overall performance of geological disposal concepts. It also enables the calculation of chemical reactions within both fractures and the rock matrix, which will be described in more detail in the next chapter.

Concentrations of salt may be described in one of three different ways within ConnectFlow:

- As a mass fraction c (also known as the salinity or mass concentration) of a chemical species i which is simply given by the mass of the species M_i divided by the total mass of water M_{wat} and all the m chemical species M_j.

  $$c_i = \frac{M_i}{M_{wat} + \sum_{j=1,m} M_j}$$

- As a volume concentration C of a chemical species i which is simply given by the mass of the species M_i divided by the volume of the solution.

  $$C_i = \frac{M_i}{V}$$

  The fluid density ρ of the solution can be used to convert to a mass fraction if required.

- Using a set of defined compositions of chemical species, known as reference waters. In this case a set of n reference waters is specified, each of which has a fixed composition of m different chemical species. The mass fraction of an individual chemical species i in a mixture of reference waters is given by the fraction[1] of each reference water, F_w, multiplied by the mass fraction of species i within that reference water $c_{i,w}$.

  $$c_i = \sum_{w=1,n} F_w c_{i,w} = \sum_{w=1,n} \left(\frac{F_w M_{i,w}}{M_{wat} + \sum_{j=1,m} M_{j,w}} \right)$$

  ConnectFlow calculates the fraction of each reference water and then the concentrations of the components are inferred from the above equation. Note

[1] It is also possible to define reference waters by volume concentration.

that the fraction of each reference water varies between zero and one and the total fraction of all reference waters sums to one.

$$\sum_{w=1,n} F_w = 1 \tag{4-1}$$

Reference waters are beneficial when groundwater composition can be inferred from mixtures of a small number of waters of identifiable origins, for example glacial melt water, meteoric water or sea water, and when the water sources have a larger number of dissolved solute species (i.e. when m>n). In that case it is more efficient to transport the *n* reference waters rather than the *m* chemical species and save computational time. If there are no clearly defined reference waters in the system or if hydrogeochemical calculations are required, then reference waters are not appropriate, and the concentrations of each solute must be individually calculated. Note that reference waters can still be used to specify an initial condition or boundary condition even if the calculation transports each solute individually.

The solute transport calculations reported in previous chapters are effectively reference water calculations with two reference waters, one fresh and one saline. ConnectFlow calculates the concentration of the saline reference water and then infers the concentration of the fresh reference water using Equation (4-1) above. This chapter demonstrates calculations with two or more reference waters. The transport of individual components will be demonstrated in the following chapter, where this is specifically required for hydrogeochemical calculations.

4.2 Mathematical representation of solute transport in a DFN

The existing equations for transport of a saline reference water (excluding rock matrix diffusion) in a ConnectFlow DFN model (Wood, 2018) are:

$$\frac{\partial(e_t\rho)}{\partial t} + \nabla\cdot(\rho\vec{q}) = 0, \tag{4-2}$$

$$\frac{\partial(e_t\rho c)}{\partial t} + \nabla\cdot(\rho\vec{q}c) = \nabla\cdot(e_t\rho D\cdot\nabla c) \tag{4-3}$$

$$\vec{q} = \frac{e^3}{12\mu}\left(\nabla P_R - (\rho-\rho_0)\overrightarrow{g_f}\right) \tag{4-4}$$

$$\frac{1}{\rho} = \frac{1-c}{\rho_0\left(1+\alpha_f\left(P_T - P_{T_0}\right)\right)} + \frac{c}{\rho_s\left(1+\alpha_s\left(P_T - P_{T_0}\right)\right)} \tag{4-5}$$

The variables referred to here are:

- e_h (m) is the effective hydraulic aperture of a fracture, which may vary within the fracture and between fractures;
- e_t (m) is the transport aperture of a fracture, i.e. the effective aperture of a fracture accessible to mobile water, which may vary within the fracture and between fractures;

- c (-) is the fraction of the saline water and $(1 - c)$ is the fraction of fresh water.
- ρ (kg m^{-3}) is fluid density;
- ρ_s (kg m^{-3}) is the saline fluid density; ρ_0 is the reference fluid (fresh water) density;
- α_s (m^2 N^{-1}) is the compressibility of saline water; α_f is the compressibility of fresh water;
- P_T (N m^{-2}) is the local total pressure;
- P_{T0} (N m^{-2}) is the reference pressure;
- μ (kg m^{-1} s^{-1}) is fluid viscosity (constant);
- P_R (N m^{-2}) is the local residual pressure: $P_R = P_T - P_{T0} + \rho_0 g(z - z_0)$, where g is the magnitude of gravitational acceleration, z is the elevation and z_0 is the reference elevation.
- $\vec{Q}$ (m^2 s^{-1}) is the flow through the fracture per unit width of the fracture.
- t (s) is time;
- D (m^2 s^{-1}) is the dispersion tensor (including contribution from diffusion within the mobile water system of fractures or equivalent pores);
- ∇ is the two-dimensional gradient operator within the fracture;
- $\overrightarrow{g_f}$ (m s^{-2})is the acceleration due to gravity in the plane of the fracture.

Transients are typically calculated using a fully implicit scheme to avoid unphysical oscillations, although a Crank-Nicolson scheme is also available. Where steady-state calculations are performed, the derivatives with respect to *t* are zero.

These equations are extended to transporting n reference waters by using Equation (4-3) to calculate the fraction c_w of $n - 1$ reference waters,

$$\frac{\partial(e_t \rho c_w)}{\partial t} + \nabla \cdot \left(\rho \vec{Q} c_w\right) = \nabla \cdot (e_t \rho D \cdot \nabla c_w) \qquad (4\text{-}6)$$

and then the concentration of the remaing reference water is inferred from Equation (4-1). When transporting mass-fractions of individual solutes, rather than reference waters, the transport equations have the same form as Equation (4-6). However, in this instance all the n solutes must be calculated using this equation rather than $n - 1$.

The way the density and viscosity are calculated is significantly different between the older single-component solute transport algorithm and the updated algorithm for transporting multiple reference waters. In the former case, the density is calculated using Equation (4-5) and the viscosity is assumed constant. In the latter case, the density and viscosity are calculated according to an empirical method described by Kestin et al. (1981). This method calculates the density and viscosity according to the total mass of dissolved solids of all species as well as the pressure and the temperature (a fixed temperature distribution can be specified at the start of the calculation). The expression was originally derived using NaCl, but it is considered a reasonable approximation for multiple salt species. This mirrors the approach used for ConnectFlow CPM calculations. The rock matrix diffusion algorithm has also been extended to work for an arbitrary number of chemical species.

There are some limitations to the approach, for example heat transport and unsaturated groundwater flow are not considered. Additionally, the dispersion lengths and intrinsic

diffusion coefficients are assumed to be the same for all species (although they can vary depending on the host rock).

4.3 Implementation of multi-component solute transport in ConnectFlow

While it is possible to calculate the pressure field and all the concentrations for multi-component solute transport using standard Newton-Raphson iterations, in practice this is likely to prove computationally expensive. This is particularly true given a large number of solute variables. To mitigate these performance issues, a sequential iteration algorithm has been implemented in the DFN case. The effectiveness of this approach has previously been demonstrated in ConnectFlow CPM calculations.

In sequential iteration, the algorithm iterates through a list of variables, calculating each as though it were independent of all the others. For each variable, it will solve the relevant equations while holding all other variables constant[2] (in time). Typically, this means solving for the pressure, assuming static solute concentrations, and then solving for the concentration of solute, assuming a static pressure field. Once all the variables have been updated, a convergence check is applied to determine the relative change of all variables. If there is a significant change then the variables are updated in the same sequence repeatedly until a convergence criterion is met. This repetition of the sequence is known as "outer iteration". Additionally, an automatic time-stepping scheme can be used to reduce the time-step and repeat a given time-step if the criterion is not met once all the outer iterations have been completed in a transient calculation.

While a coupled calculation typically has two levels of iteration (Newton-Raphson iteration and iterative linear solve), sequential iteration has up to four levels (Outer iteration, sequential iteration over the pressure and concentration variables, Newton-Raphson iteration and linear iteration). Figure 4-1 provides an example for three reference waters.

The advantage of using sequential iteration is that each linear equation calculation is more tractable and requires fewer memory resources from the computer. Sequential iteration allows a solution to be found without these memory constraints. Additionally, the efficient and parallelisable GMRES-AMG linear solver can be used for single variable calculations, whereas the slower and sequential GMRES-ILU linear solver typically has to be used for multi-variable calculations. This provides a significant extra benefit when using sequential iteration.

In the sequential iteration algorithm, certain variables may be updated without a full finite element calculation. For example, Equation (4-1) states that the fractions of reference waters must add to one. Thus, if all reference waters except one have been calculated, the last is trivially inferred. Density and viscosity, where they are used as variables, may also be calculated algebraically as part of the sequence, based on the components present in the water at a given location, using the method described in Kestin et al. (1981).

---

[2] It is actually possible to solve two or more variables simultaneously while using the sequential iteration algorithm. This can be used to allow very strongly coupled variables to be solved together, while other less coupled variables are solved sequentially.

Where possible, an effort has been made to ensure that the DFN implementation is similar to the CPM implementation of the same functionality in ConnectFlow. This allows easy transfer of equivalent concepts between models with different kinds of rock. For example, in CPM multi-component solute transport a temperature variable is always specified, even when heat transport has not been specified. In the same way, the temperature variable is always included in DFN multi-component solute transport. A static but spatially varying temperature distribution may therefore be applied and is considered in density and viscosity calculations. However, heat transport calculations are not available in DFN models at this time.

```
Time-step Loop
   Newton-Raphson Loop
       Assemble flow and transport equations
       GMRES-ILU solve for pressure + reference
       waters 1 and 2
   End Newton-Raphson Loop
   Reference water 3 implied
End Time-step loop
```

```
Time-step Loop
   Outer iteration loop
      Newton-Raphson Loop
         Assemble flow equations
         GMRES-AMG solve for pressure
      End Newton-Raphson Loop
      Assemble transport equation 1
      GMRES-AMG solve for reference water 1
      Assemble transport equation 2
      GMRES-AMG solve for reference water 2
      Reference water 3 implied
   End Outer iteration Loop
End Time-step loop
```

Figure 4-1. *Comparison of Standard Iteration (top) with Sequential Iteration (bottom) for a three reference water calculation. Note that the Sequential Iteration algorithm has up to four levels of iteration (for each time-step): outer iteration, iteration over variables, Newton-Raphson iteration (required if one of the variable solves is non-linear) and finally the iterations of the linear solver (GMRES-ILU or GMRES-AMG). The concentration of the third reference water is implied from other two reference waters in both cases.*

4.4 Verification

A series of tests have been performed for multi-component solute transport within a DFN, with increasing complexity. These compare the DFN results of multi-component calculations with those from single-component DFN calculations. Additional comparisons are made with equivalent CPM models.

4.4.1 Single-fracture cases

The single fracture model specified in Subsection 3.4.1 has been reintroduced to carry out several simple verifications of both multi-component solute transport and also the sequential iteration method (in a DFN).

Testing sequential iteration using single-component solute transport

The first single fracture test compares a calculation using sequential iteration against an equivalent calculation using standard iterations where all variables are solved for simultaneously. Both cases employ single-component solute transport. Two versions, one including RMD and one without, were calculated in each case. Table 4-1 gives the physical parameters used for this test case.

Table 4-1. *Parameters used for the single-fracture case with single-component solute transport.*

Parameter	Symbol	Value
Salt diffusion coefficient	D_{salt}	10^{-9} m^2/s
Longitudinal dispersion length	$l_{D_{long}}$	100 m
Transverse dispersion length	$l_{D_{trans}}$	10 m
Kinematic porosity (CPM)	ϕ_f	0.01
Transport aperture (DFN)	e_t	0.01 m
Density of fresh water	ρ_{wat}	998.217 kg/m^3
Density of saline solution	ρ_{sol}	1026.08 kg/m^3
Matrix porosity	α	0.3
Matrix diffusion coefficient	D_i	$5 \cdot 10^{-11}$ m^2/s
Fracture Area per unit Volume (CPM)	σ	2.0 m^2/m^3
Matrix diffusion length	w_{max}	0.495 m
Number of RMD cells	n_{fv}	5
RMD cell lengths	w_i	0.099 m
Storativity (DFN)	S_{DFN}	0
Specific storage coefficient (CPM)	S_{CPM}	0 m^{-1}

The time-step is 10^7 seconds in the simulated period up to 10^9 seconds, it then increases to 10^8 seconds in the period up to 10^{10} seconds. (The longer time-step, used during the second period, was necessary to efficiently model the extended time period over which the transport occurred when RMD was used). In this simple test case, relatively few outer iterations were required (four or less) at each time-step for the sequential iteration

calculation. A similar number of Newton-Raphson iterations were required for the case where all variables were solved simultaneously. In more complicated models, it is expected that more outer iterations would be required or smaller time-steps when using sequential iteration.

Dirichlet boundary conditions are imposed at x=0 m with a head of 50 metres and a saline mass fraction of 1.0. At x=10,000 m, a head of 0 metres is imposed and an outflow boundary condition is applied for the solute. The initial saline mass fraction is set to zero throughout the block.

Figure 4-2 presents the mass fraction of saline water at x = 5000 metres for each calculation. It is apparent that the results with sequential iteration are a good match to the standard calculation where all variables are solved for simultaneously. This is apparent both with and without RMD.

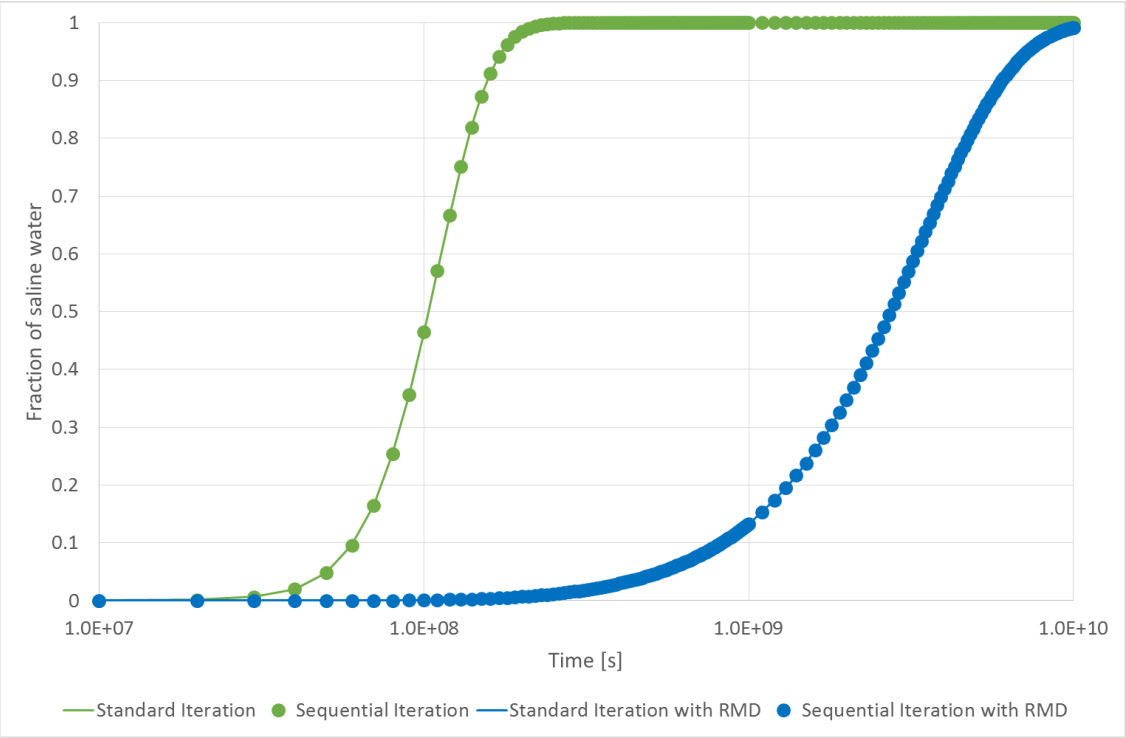

Figure 4-2. *Comparison of a standard DFN solve and sequential iteration DFN solve, for calculations with and without RMD. The green line is the standard solve without RMD and the green circles are the corresponding sequenital iteration solve. The blue line is the standard solve with RMD and the blue circles are the corresponding sequential iteration solve. The results using sequential iteration closely match the standard solve.*

Table 4-2. *Properties of the reference waters used in the 2-reference water case, assuming a temperature of 20°C and atmospheric pressure, as reported by ConnectFlow. Note that the Density and Viscosity will vary with temperature and pressure.*

Parameter	Salinity [g/kg]	Density [g/L]	Viscosity [Pa·s]
Brine	38.977	1026.0	$1.0607 \cdot 10^{-3}$
Dilute	0.0	998.22	$1.0020 \cdot 10^{-3}$

Testing multi-component against single-component solute transport

The second single fracture case compares the same single-component solute transport model with an equivalent multi-component case with two reference waters. In this case, there is one saline reference water and one dilute reference water. The proportion of the solution that is the saline reference water is equivalent to the concentration of the saline water in the single-component solute transport case and the dilute water should make up the remainder. A constant temperature of 20°C is applied and the salinities of the two reference waters are chosen such that their densities matched the equivalent densities in the single-component model (at atmospheric pressure). Additionally, the viscosity of the dilute reference water is equivalent to the viscosity used in the single-component model. Importantly, the multi-component solute transport case allows the viscosity to vary, whereas the single-component case does not, so it was not possible to match the viscosity of the saline reference water as well. Given that groundwater velocity is inversely proportional to viscosity (if all other variables are kept constant), this may have a noticeable impact on the transport. The viscosities, salinities and densities of the two reference waters are given in Table 4-2.

RMD is not included in this calculation, and the time-steps in this case were kept at a constant of size 10^7 seconds throughout the duration of the simulation, which was 10^9 seconds.

This multi-component reference water case is equivalent to the single-component solute transport case, but there are some differences in the two approaches (this is discussed in detail earlier in this chapter). Significantly, the density and viscosity are functions of salinity, temperature and pressure in the multi-component calculation; while the viscosity is constant and the density only varies with salinity in single-component transport. This has a noticeable impact on the transport. To isolate these effects from the tests, the equivalent calculations have been carried out in a CPM as well. The DFN calculations use sequential iteration while the CPM calculations use standard Newton-Raphson iterations.

Figure 4-3 presents the mass fractions at $x = 5000$ metres in each calculation. It is apparent that the DFN results with sequential iteration are a good match to the CPM results using standard Newton-Raphson iterations. It is also clear that the different approaches to the calculation of density and viscosity have created a small difference in the speed at which the saline water moved across the fracture.

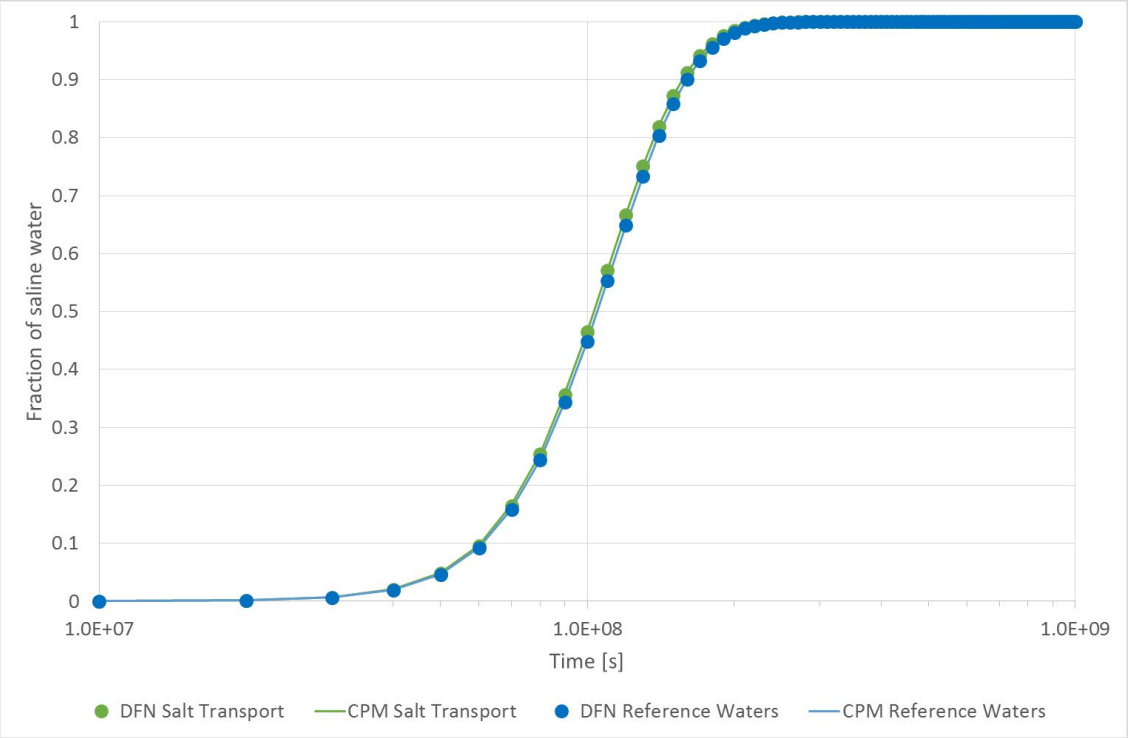

Figure 4-3. *Comparison of calculations using the single-component solute transport method (green circles for DFN, green lines for CPM) and the reference water method (blue circles for DFN, blue lines for CPM); note the logarithmic time scale on the X axis. The reference water calculations give slightly different results to the single-component solute transport calculations (for both CPM and DFN) because they use different methods for calculating density and viscosity (see text).*

Testing multi-component solute transport with three reference waters

The third single fracture test case demonstrates transport of three reference waters within a DFN, namely Brine, Meteoric and Glacial[3]. The salinities, densities and viscosities of the waters are given in Table 4-3.

The model initial conditions are a mixture of 25% Brine and 75% Meteoric water. The boundary conditions have one side of the fracture with a head of 50 metres, and an inflow of a mixture of 25% Meteoric water and 75% Glacial water; the other side of the fracture has zero head and a fixed concentration of 100% Brine solution. An equivalent CPM model was also constructed.

It is anticipated that, at a given position in the middle of the fracture, the proportion of waters would change over time to eventually match the composition of the inflow waters, once a steady state had been reached. The only brine in the model should arise from diffusion against the flow, from the outflow end of the fracture. Figure 4-4 presents a comparison between the DFN and CPM cases and the results were as expected.

[3] Note that Brine does not have the same properties as in the two reference water case.

Table 4-3. *Properties of the reference waters used in the 3-reference water case, assuming a temperature of 20°C and atmospheric pressure, as reported by ConnectFlow. Note that the Density and Viscosity will vary with temperature and pressure.*

Parameter	Salinity [g/kg]	Density [g/L]	Viscosity [Pa·s]
Brine	34.964	1023.1	$1.0539 \cdot 10^{-3}$
Meteoric	0.20153	998.36	$1.0022 \cdot 10^{-3}$
Glacial	0.0	998.22	$1.0020 \cdot 10^{-3}$

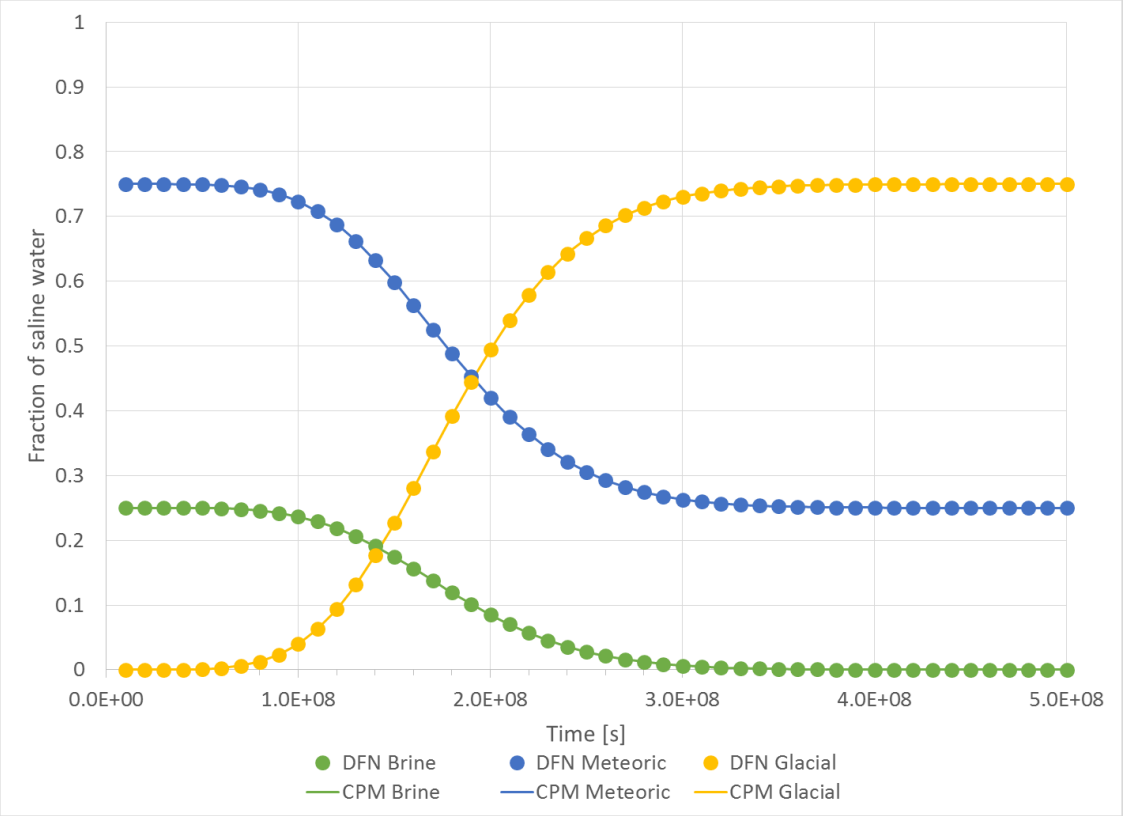

Figure 4-4. *Comparison between DFN (circles) and CPM (lines) of proportions of reference waters in the system in a three-reference water case. The reference waters each have a differerent composition and density.*

4.4.2 Olkiluoto site-scale model

In this section, the meteoric water flushing model for Olkiluoto is revisited to test the DFN implementation of multi-component solute transport on a large stochastic fracture network. The verification is accomplished by reproducing the DFN single-component solute transport results from Chapter 3 using the updated multi-component solute transport method.

Initial calculations revealed that there was a significant coupling between the transport and flow solves. This means the transport of the salt changes the density significantly enough to affect the pressure over short time scales (less than a year). Using sequential iteration in such cases is difficult since the pressure and salinity are updated separately, which can result in the two being inconsistent unless a small enough timestep is used. For this reason, the multi-component solute transport calculations were performed using standard Newton-Raphson iterations.

Two reference waters are used for the multi-component calculations. This enabled a direct comparison with the single-component solute transport results in Chapter 3 and it also improved tractability, given that sequential iteration is not suitable. The salinity of the two reference waters is chosen such that the densities match the respective saline and dilute waters used in the single-component transport calculations of Chapter 3. The viscosity of the two reference waters is governed by their salinity, temperature and pressure. The properties of the two reference waters are given in Table 4-4.

Table 4-4. *Properties of the two reference waters for the Olkiluto site scale simulation. The asterisk denotes that this property is taken at standard temperature and pressure and will vary depending on temperature and pressure.*

	Description	**Dissolved* Solids (g/l)**	**Density* (g/l)**	**Viscosity* (Pa.s)**	**Salinity (g/kg)**
Reference Water A	Brine	30.47 (Na) 47.03 (Cl)	1051.4	$1.128 \cdot 10^{-3}$	73.71
Reference Water B	Meteoric	0.950 (Na) 1.470 (Cl)	999.9	$1.005 \cdot 10^{-3}$	2.420

A static temperature distribution is used for the multi-component calculation. This varies linearly from 6°C at sea level to 25.7°C at 1400m below sea level. Rock matrix diffusion is included. Other properties are equivalent to those used in the models described in Chapters 2 and 3.

The current model provides the following improvements over the single component solute transport calculations of Chapter 3:

- The density varies with temperature and pressure rather than just salinity.
- The viscosity varies with temperature, pressure and salinity rather than being constant.

The viscosity of water varies by more than 65% over the temperature range specified in the model and the transmissivities of the fractures will change accordingly.

The results for the multi-component transport calculation (including an equivalent CPM model) are given in Figure 4-5. Some minor differences are seen compared with the equivalent single component calculations in Figure 3-9, and these are most likely due to the different treatment of density and viscosity. As was the case in Chapter 3, there are

some differences in concentrations between the DFN and CPM at 4000 AD. The latter is probably due to additional connectivity inherent in an ECPM model.

In conclusion, the multi-component solute transport method for a DFN has been shown to function correctly in so far as it reproduces equivalent ECPM results in a simple fracture. In larger, more complicated discrete fracture networks, some differences between ECPM and DFN representations can be seen and these are likely due to the approximations made in the ECPM representation.

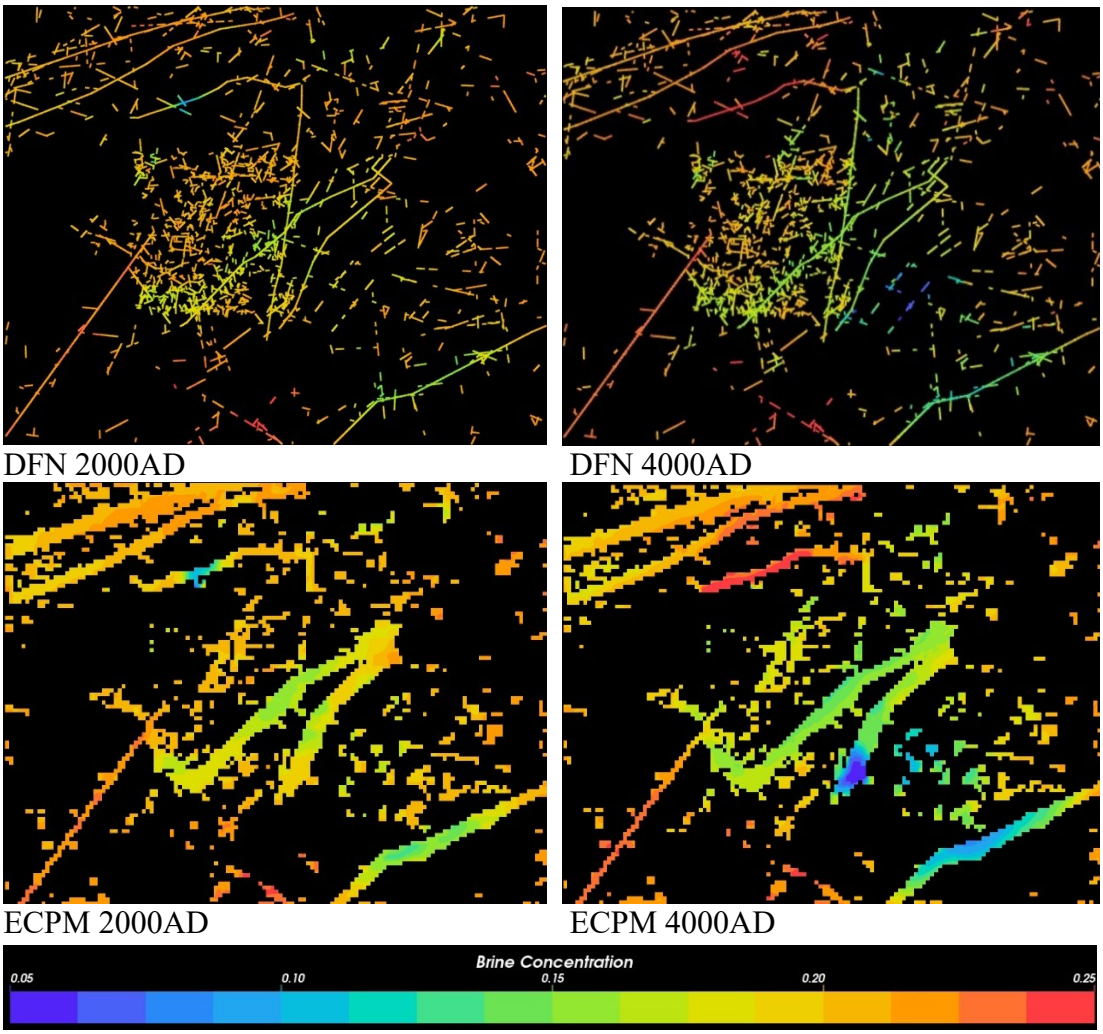

Figure 4-5. *Evolution of salinity over 2000 years at the Olkiluoto site for a two reference water multi-component solute transport calculation. ECPM and DFN models are shown and both include RMD. The horizontal slices are at −400m depth.*

5 REACTIVE TRANSPORT IN DFN MODELS

5.1 Introduction

Reactive transport has previously been implemented in ConnectFlow for CPM models, as described in Joyce et al. (2014a). This is accomplished using an interface to PHREEQC (Charlton and Parkhurst 2011) which is an extensively used geochemical software product. PHREEQC is capable of simulating a wide range of chemical reactions, including equilibration of aqueous solutions with minerals, ion exchanger materials, surface complexes, solid solutions and gases. It can also simulate kinetic non-equilibrium reactions. PHREEQC is freely available in the form of a software library called iPhreeqc (Charlton and Parkhurst 2011), which is the product that ConnectFlow interfaces with. ConnectFlow has now been upgraded to allow DFN calculations to access the geochemical capabilities of PHREEQC via the same interface and library. Future upgrades to the library and/or interface will therefore become available for use by both DFN and CPM calculations.

5.2 Background

The types of reactions that are available to ConnectFlow via the iPhreeqc library are described briefly below.

5.2.1 Equilibrium reactions

The most common type of chemical reaction in a hydrogeological setting is the reaction of ions in aqueous solution with rock minerals. Reactions that are faster than the characteristic time of groundwater flow can be considered to be at equilibrium. In this case, the minerals are treated as being in equilibrium with solutes in aqueous solution. For the groundwater evolution of regional-scale models, with timescales over thousands of years, many of the reactions of interest can be considered to be at equilibrium. Typical equilibration reactions considered in groundwater chemistry are the dissolution or precipitation of pyrite, calcite and quartz (respectively given below):

$$4FeS_2 + 14O_2 + 4H_2O \longleftrightarrow 4Fe^{2+} + 8SO_4^{2-} + 8H^+$$

$$4Fe^{2+} + O_2 + 4H^+ \longleftrightarrow 4Fe^{3+} + 2H_2O$$

$$SiO_2 + 2H_2O \longleftrightarrow H_4SiO_4$$

For fractured rock, minerals may be present on the surfaces of the fractures or they may be located within the rock matrix. The fracture coating minerals may be the same as or different to those in the rock matrix (Smellie 2014). Likewise, there may be differences in the groundwater composition in the fractures and the rock matrix at any point in time. There will also be minerals associated with the rock mass itself. For the Forsmark site, the main fracture minerals are calcite, chlorite and pyrite, plus clay minerals and a small amount of hematite (Löfgren and Sidborn 2010). The rock matrix is granitic and so the associated minerals will be silica and silicates, such as quartz. Olkiluoto has similar minerals (Posiva 2009, Smellie 2014).

Reactions need not involve existing minerals on the fracture surfaces. For example, sulphates dissolved within groundwater can be transformed into sulphides under reducing conditions.

5.2.2 Ion exchange reactions

A further category of hydrogeochemical reaction are ion exchange reactions. These are reversible equilibrium processes that occur between ions held at the surface of a mineral and ions in aqueous solution. These reactions affect the water composition by swapping one ion for another in aqueous solution. Ion exchange properties are seen in some minerals, particularly clays, such as zeolites and montmorillonite. Clays occur on fracture surfaces at both Forsmark (Löfgren and Sidborn 2010) and Olkiluoto (Posiva 2009) and so there is potential for ion exchange reactions in the fractured rock at these sites. The bentonite used in repository backfill and around the radioactive waste canisters is also an ion exchanger. Although ion exchange reactions were not considered at the regional-scale for SR-Site due to a lack of data (Salas et al. 2010) they have been considered for Olkiluoto with an illite-like exchanger (Trinchero et al. 2014).

5.2.3 Surface complexation

Surface complexation occurs when ions in aqueous solution are adsorbed on a mineral surface by the formation of complexes. There are two "levels" of surface complexation. The first is known as the "Inner-sphere" where an ion binds directly to a specific site on the surface and can then be approximated as part of that surface. The second level is known as the "Outer-sphere" where the ion only binds electrostatically to the surface and forms a diffuse layer with other ions adjacent to the surface. The species on the surface of the mineral may be anionic, cationic, or neutral and more than one of these species may be present on a surface. PHREEQC supports three types of surface complexation model:

- Generalized two-layer model
- Two-layer model that explicitly calculates the diffuse-layer composition
- Non-electrostatic surface-complexation model

5.2.4 Kinetic reactions

In natural systems, redox element speciation is often out of equilibrium with speciation of other redox-sensitive elements and with measured redox potentials (e.g. Sigg 2000). These are important reactions with relevance for repository safety, including aluminosilicate weathering, illitisation of bentonite, clay hydrolysis, cement leachate reactions and microbially mediated processes that are nutrient limited. The slow rate of these reactions means they may occur on timescales that are significant compared to the transport timescales within regional scale groundwater models and a timestepping scheme is necessary.

5.3 Implementation

The ConnectFlow interface to the iPhreeqc library is in the form of a series of subroutines that allow text-based commands to be passed to PHREEQC using the PHREEQC command language. This allows the full capability of the PHREEQC software to be

available via the library. The interface also allows the state of the system to be updated and selected quantities to be output.

The list of reactions that can occur and the mineral phases available for a given calculation are specified via a thermodynamic database, which is an input to the iPhreeqc library. Any PHREEQC-compatible thermodynamic database file can be specified for the chemical reaction calculations.

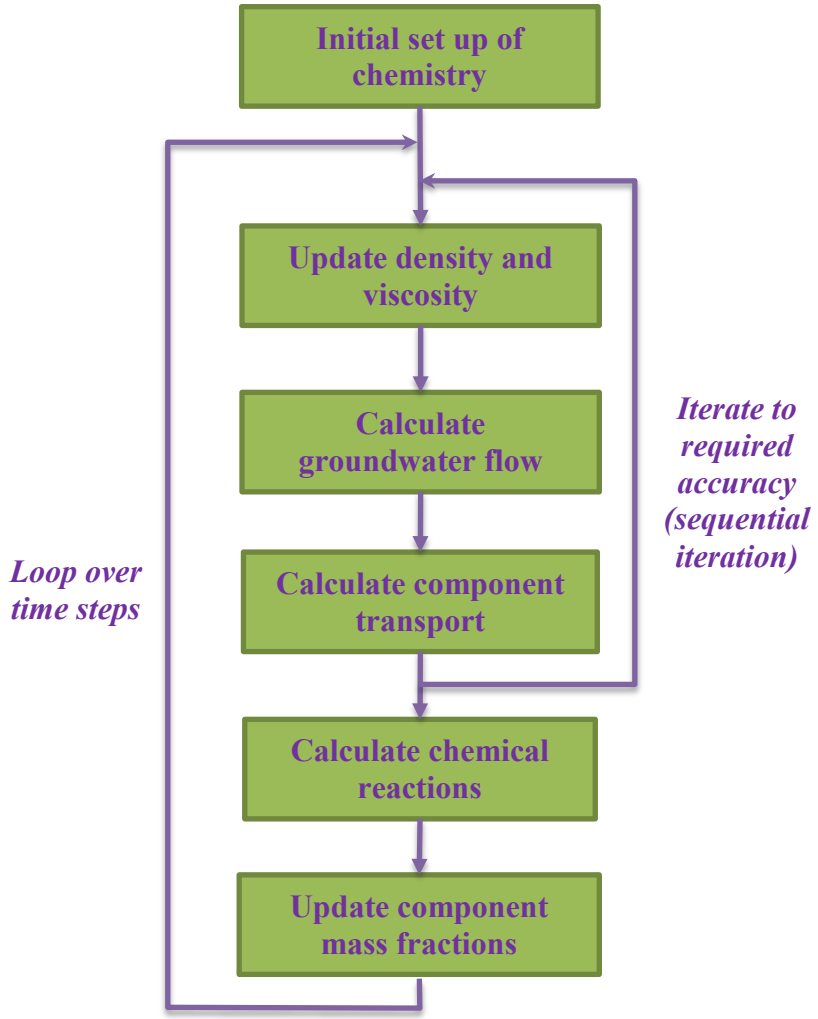

Figure 5-1. *Flow diagram of reactive transport within ConnectFlow for equilibrium reactions. For kinetic reactions the workflow is the same but the chemical reactions are calculated using a timestepping routine within iPhreeqc. The total duration of these timesteps is equal to the ConnectFlow transport timestep.*

The steps ConnectFlow performs to calculate multi-component solute transport with rock matrix diffusion and chemistry within ConnectFlow are summarised in Figure 5-1 (assuming equilibrium chemistry reactions and sequential iteration). ConnectFlow solves the flow and transport equations at the start of each timestep. This is typically carried out via sequential iteration. In that iteration, the density and viscosity are updated first to ensure they are consistent with the current salinity, pressure and temperature. Next the flow is calculated and finally the solutes are transported. This loop is repeated until the

timestep is resolved to the required accuracy. Once this is done, the aqueous solution at each location in the model where chemical reactions are being carried out is then updated with the mass fractions of components modified due to the chemical reaction calculations in iPhreeqc. The values of pH and pe are also updated at each location.

The process for kinetic reactions is very similar, except the calculation of the chemical reactions within iPhreeqc has its own internal timestepping scheme. These internal timesteps run for the same duration as the ConnectFlow transport timestep. The PHREEQC timestep length and scheme are specified in the ConnectFlow data set.

PHREEQC expresses all chemical equations in terms of master species. It is typical to use one master aqueous species associated with each element, e.g. one species covers both valence states Fe^{2+} and Fe^{3+}, but there is also the option to have one master species for each valence state. Therefore, there is one transported component in ConnectFlow for each master species specified in the PHREEQC thermodynamic database that defines the reactions of interest. Only those master species present in the groundwater under consideration or are produced as a consequence of the chemical reactions need to be included for transport. However, to fully define the chemical state of the system, three additional components must always be defined, namely H (total hydrogen not included in water molecules), O (total oxygen not included in water molecules) and E (charge balance). It is necessary to know the quantity of H and O, since they are constituents of some species involved in chemical reactions, but since the quantity included in H_2O is known from the quantity of water, it is not necessary to transport the H and O included in water molecules and it is more accurate not to do so. The charge balance, E, should be zero for a physical system, but due to numerical rounding it is typically in the range $1.0 \cdot 10^{-18}$ to $1.0 \cdot 10^{-12}$. ConnectFlow transports E to prevent numerical charge imbalances arising from the chemistry calculations.

As mentioned in the previous chapter, ConnectFlow has the ability to transport solutes in a number of ways, including transport of reference waters and transport of chemical components. Previous regional-scale palaeo-climate simulations have been expressed in terms of the transport of reference waters (Follin 2008, Joyce et al. 2010, Hartley et al. 2012, 2013). This is convenient, since each reference water represents water of a particular origin, e.g. meteoric or glacial, and the composition of the groundwater at any point is expressed in terms of the mixing of fractions of the reference waters. However, the reference water approach is not appropriate when considering chemical reactions. This is because the concentration of any individual component at any point may change as a result of the reactions, so the composition of the reference water cannot then be maintained. Therefore, when carrying out chemical reactions, individual chemical components are transported within ConnectFlow. Each component is transported separately and its mass fraction can be individually updated as a result of chemical reactions. Nonetheless, it can be convenient to be able to define reference waters and use them in turn to define calculation of initial conditions and boundary conditions; these will be converted to components as required before the calculation actually takes place. Note that ConnectFlow expresses the transported quantities in terms of mass fractions, i.e. the mass of each solute (kg) per kilogram of solution (kg_s), while PHREEQC expresses quantities in terms of molalities, i.e. moles of each solute (mol) per kilogram of water (kg_w). Therefore, when concentration data is exchanged between ConnectFlow and PHREEQC it is necessary to convert between the two quantities. This requires molar

masses for the master species, which are obtained from the thermodynamic database specified.

The implementation in the DFN is very similar to the existing CPM implementation: the transport calculation is performed at the start of each timestep and, upon completion, the chemical reactions at each ConnectFlow solution node are calculated using the iPhreeqc library. Note that, in DFN calculations the solution nodes are defined at fracture intersections, rather than on the individual finite elements within each fracture.

All reactive transport scenarios in the CPM are also available in the DFN. These can be used to calculate and output "Smart K_d" values (that vary as a function of groundwater composition) for radionuclide transport calculations (radionuclide transport is not yet implemented in the DFN, but it is a likely future development).

5.3.1 Rock matrix diffusion

The finite volume rock matrix diffusion method described in Chapter 3 can be extended to calculate chemical reactions within the rock matrix. This is implemented in the DFN by noting the chemical composition of the porewater and rock minerals within each of the finite volume cells representing the matrix and then utilising iPhreeqc to carry out reactions in each cell. The matrix reactions are carried out at the end of each timestep in exactly the same manner as the reactions in the fractures themselves. Note that the temperature is needed for the chemistry calculations and this is assumed to be the same in the rock matrix as it is in the fracture. This ignores any effect from heat transport within the groundwater (a good assumption in most practical cases).

5.3.2 Mineral Quantities

Mineral quantities are assigned a uniform quantity across the model, which defaults to 10.0 mol/kg_w (the PHREEQC default), if not specified. If the initial quantity of a mineral phase is set to zero then it is considered to be a secondary mineral, in which case it cannot initially dissolve, but may precipitate (and possibly subsequently dissolve) as the result of a chemical reaction.

If the quantities of the minerals change as a result of chemical reactions then any variable values associated with the minerals are updated accordingly. However, the mineral quantities are also maintained internally by iPhreeqc.

Note that minerals quantities may not be uniformly distributed throughout a geological system but may vary, for example by rock type or depth. In CPM calculations it is possible to define these quantities as variables, but this has not as yet been implemented for DFN calculations.

5.4 Testing

A series of tests have been performed for reactive transport within a DFN, with increasing complexity. These validate the DFN implementation of hydrogeochemistry by using a comparison between equivalent DFN and CPM models. These examples will also effectively test the functionality of transporting solutes by component. This was introduced in the previous chapter alongside the transport of multiple reference waters

but was not explicitly validated there. It will also check the software's ability to use defined reference waters to set initial conditions and boundary conditions when the transport is calculated by component.

5.4.1 Single-fracture cases

Single fracture test cases were carried out using a cuboid block of rock with the same parameters as the multicomponent transport example in Section 4.4.2. A sample reactive transport test was carried out, demonstrating calcite equilibration.

In each case, equivalent chemistry calculations have been performed using both the DFN and the CPM representations and additional control calculations have been carried out without reactive transport.

Calcite transport

This case involves two reference waters and their interaction with calcite. One reference water is sea water and the other a more dilute solution. Each reference water is equilibrated; and charge is balanced at the start of each calculation. This means the reference water components can be reacted (in isolation) using iPhreeqc before timestepping begins. The charge balanced composition of the reference waters is given in Table 5-1 together with its pH, pe and charge balance E. Note, the reference waters are also charge balanced for the control calculations without chemistry to ensure that each calculation started from the same initial condition.

In their initial state, the fracture and its associated rock matrix, are fully saturated with dilute water. Boundary conditions are then applied as follows: on the left-hand side a constant 100% concentration of sea water is maintained, together with a head of 50 metres; on the right-hand side a 100% concentration of dilute water is maintained, together with a head of 0 metres. Reactions take place between the chemical components dissolved in the water and calcite.

Figure 5-2 and Figure 5-3 provide comparisons of the mass fractions of carbon and chlorine respectively for CPM and DFN calculations with and without reactive transport. The concentrations are measured half way along the fracture. Figure 5-4 gives the pH of the resultant solution. In each case, there is excellent agreement between the DFN and CPM models. Due to the high pH of the system, calcite is deposited within the fracture as the sea water travels through the fracture. This reduces the aqueous concentration of carbon within the fracture when compared with the control calculation without chemistry. The concentration of chloride is not affected.

Table 5-1. *Mass fractions of components transported in the calcite transport calculation in a single fracture case after charge balancing. Values of pH and pe are only included in reactive transport calculations.*

Component	Sea	Dilute
C [kg/kg]	$2.0051 \cdot 10^{-5}$	$1.4740 \cdot 10^{-6}$
Ca [kg/kg]	$6.6906 \cdot 10^{-5}$	$4.9186 \cdot 10^{-6}$
Cl [kg/kg]	$4.0585 \cdot 10^{-3}$	$3.5449 \cdot 10^{-8}$
Na [kg/kg]	$2.5935 \cdot 10^{-3}$	$2.2990 \cdot 10^{-8}$
H [kg/kg]	$1.6246 \cdot 10^{-6}$	$1.6792 \cdot 10^{-7}$
O [kg/kg]	$7.9704 \cdot 10^{-5}$	$7.2232 \cdot 10^{-6}$
E [-]	$-1.5238 \cdot 10^{-16}$	$-2.0329 \cdot 10^{-19}$
pH [-]	7.9749	9.9097
pe [-]	−4.4486	−6.5842

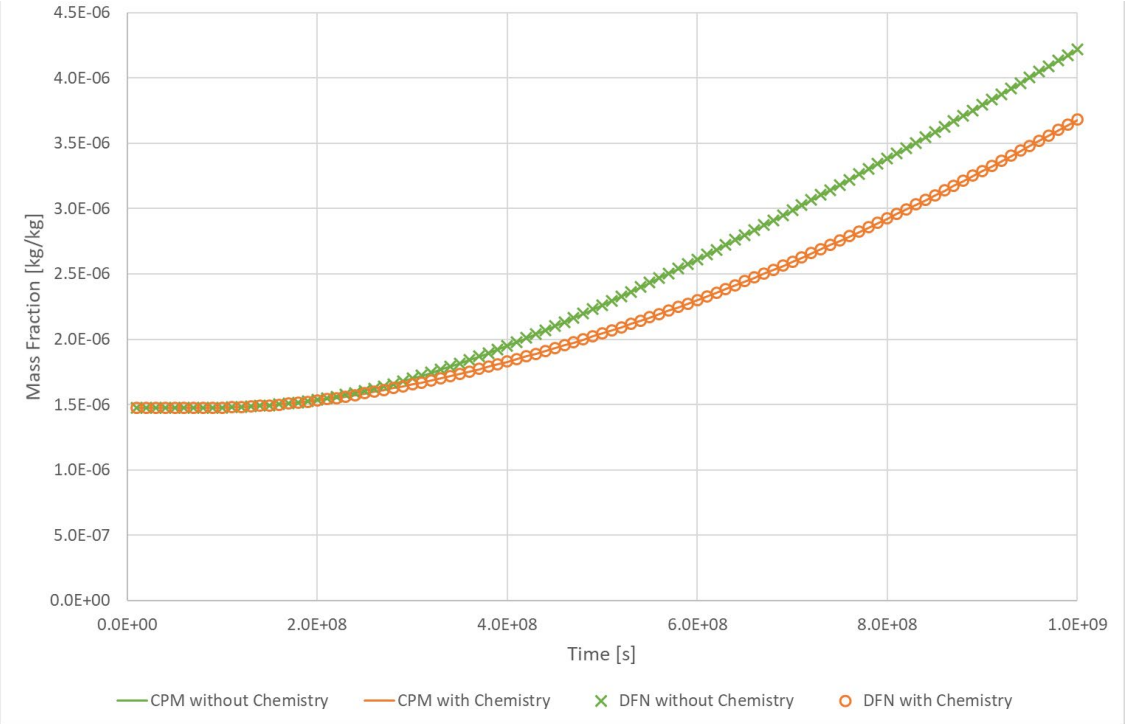

Figure 5-2. *Comparison of DFN and CPM calculations for total carbon concentration, with and without chemical reactions. The orange parts are results with chemical reactions, the green parts without; the circles are results for the DFN calculation and the lines the results for the CPM calculation.*

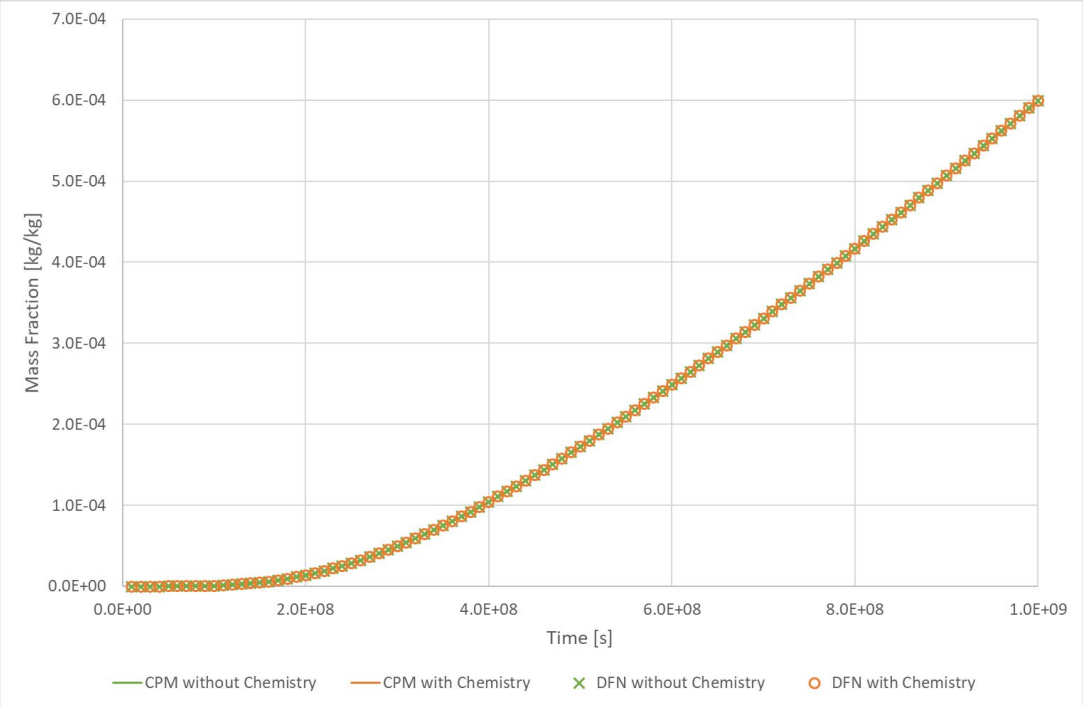

Figure 5-3. *Comparison DFN and CPM calculations for chloride concentration with and without chemical reactions. The orange parts are results with chemical reactions, the green parts without (NB. the green line/points are hidden by the orange); the circles are results for the DFN calculation and the lines the results for the CPM calculation.*

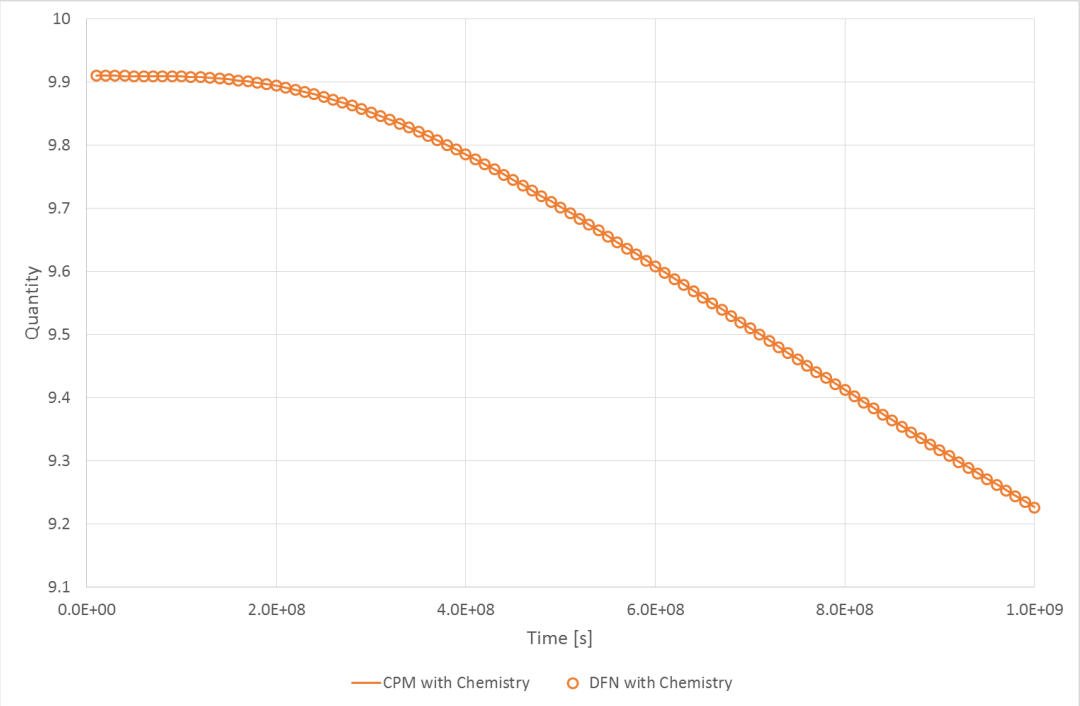

Figure 5-4. *Comparison of pH of the solution created by reactive transport in DFN and CPM calculations; the circles are results for the DFN calculation and the lines the results for the CPM calculation. The pH is not calculated in non-reactive transport.*

5.4.2 SFL repository scale model

A demonstration repository-scale model of the SFL concept has been developed, which is 1.2 km by 1.2 km and is 2.2 km deep. The vaults are located at an elevation of around –490 m but are not included in the model. The model includes random fractures larger than 200 m side length but not hydrogeological zones or repository features. The model is based on the SR-Site Laxemar Elaborated Hydro-DFN (SKB, 2013, 2016). There are around 200 fractures in total and nearly 6000 fracture tessellates. A summary of the fracture statistics is given in Table 5-2. The simulations involve the flushing of saline groundwater by dilute meteoric water over two thousand years of the temperate period. The calculations are transient and represent advection, diffusion and dispersion within the fracture volume and the density, viscosity and pressure are fully coupled. Rock matrix diffusion is also represented explicitly. To demonstrate the effect of chemistry, an equilibrium reaction with calcite is explicitly modelled. This requires the inclusion of six chemical species, carbon, chloride, calcium, sodium, oxygen and hydrogen, within the model and an additional three tracers, pH, pe and overall charge balance (E).

The key physical properties of the model are given in Table 5-3. The longitudinal dispersion length, at 60 m, is slightly larger than the tessellation length of the fractures. The transverse dispersion length has a smaller size of 20 m. The boundary conditions applied to the model are summarised in Table 5-4. The initial value boundary conditions fix the boundary condition equal to the initial condition throughout the duration of the simulation.

Table 5-2. *Fracture statistics for the SFL DFN demonstration model.*

Property	Value	Units
Number of fractures	193	
Number of tessellates	5777	
Total P_{32}	$3.95 \cdot 10^{-3}$	m^{-1}
Tessellation length	50	m

Table 5-3. *Summary of physical properties for the SFL demonstration model.*

Property	Value	Units
Saline diffusion coefficient	$1.0 \cdot 10^{-9}$	$m^2\ s^{-1}$
Saline longitudinal dispersion length	60.0	m
Saline transverse dispersion length	20.0	m
Tortuosity	1.0	–

The initial conditions have been taken from the results of a transient regional-scale ECPM simulation of the SFL site at 2000 AD (SKB 2016). At this time, the distribution of salinity increases from the top of the model to the bottom and there is some penetration of meteoric water at the repository depth. The groundwater composition from the regional-scale model is first imported into a steady-state flow calculation for the site-scale DFN in order to calculate a consistent pressure field. The pressure calculated and the imported groundwater composition are then used as an initial condition for the solute transport calculation. At that stage, the groundwater density is converted to an equivalent salinity as the basis for the initial conditions and boundary conditions. The initial condition for the concentration in the matrix is the same as the concentration in the fracture.

Table 5-4. *Summary of boundary conditions.*

Surface	Pressure	Concentrations
Top	Initial value	Initial value
Sides	No flow	Initial value
Bottom	No flow	Initial value

ECPM representation

Comparison is made to the results of corresponding simulations carried out using an ECPM model. This model is based on an upscaling of the same DFN using a mesh with 40 m blocks (this is distinct from the regional-scale ECPM used for the initial conditions). All the boundary conditions, initial conditions and physical properties in this ECPM model are the same as those in the DFN model. The ECPM model uses three upscaled quantities: permeability, porosity and flow wetted surface. The upscaled permeability field is compared to the DFN transmissivity in Figure 5-5.

5.4.3 SFL repository scale results

Figure 5-6 presents the simulated time evolution for the concentration of chloride ions within the SFL model described in the previous section. The plots shown are slices through the model at −490 m elevation (the centre of the repository facilities). Those on the left are calculated using the explicit DFN representation while those on the right are calculated using the ECPM representation (elements with permeability less than $1 \cdot 10^{-17} m^2$ are not shown). Three points in time are displayed and calcite reactions are included in all calculations. Note that chloride ions are unaffected by the included chemical reactions and consequently this figure provides an insight to the solute transport (and matrix diffusion) in isolation from chemical reactions.

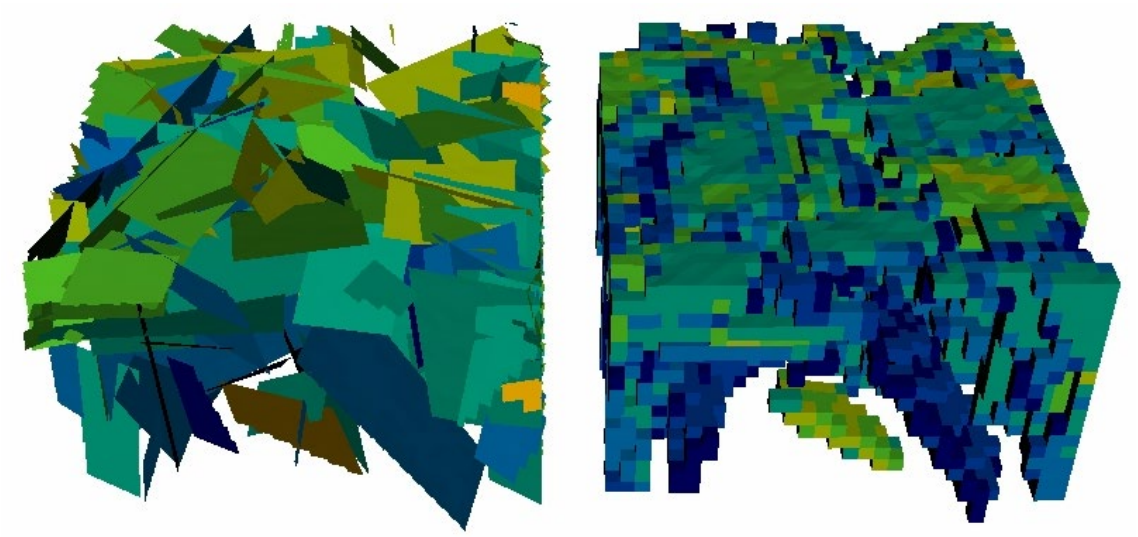

Figure 5-5. *The fracture network and the ECPM representation of it. The colours represent transimissivity and permeability respectively (dark blues correspond to low values and lighter greens and yellows correspond to higher values).*

Comparing the DFN with the ECPM representation, it is apparent the spacial variation and time variation are broadly consistent between the two. This provides further verification for the new DFN method. The ingress of fresh water is particularly apparent over the first thousand years of the simulation in the middle of the domain but then slows for the second thousand years. This may be because the interpolation used for the initial condition may have created an initial concentration profile that is too smooth and does not show variations between neighbouring fractures that might be expected in a naturally occuring fracture network.

There are some differences between DFN and ECPM. In particular, at several points the concentration in the DFN appears to be a little lower than that in the equivalent ECPM plot. It appears that the ECPM has permeable elements where there are apparently no fractures. This is not an error, but rather an artifact of the upscaling whereby the upscaled element is intersected by a fracture above or below the slice taken at −490 m.

Figure 5-7 presents the simulated time evolution for the concentration of carbon within the SFL model described in the previous section (for a DFN representation). The plots shown are slices through the model at −490 m elevation (the centre of the repository facilities). Those on the left are calculated with calcite reactions enabled, while those on the right are calculated with no chemical reactions. While chloride ions are largely unaffected by calcite reactions, inorganic carbon concentrations are significantly affected by these reactions.

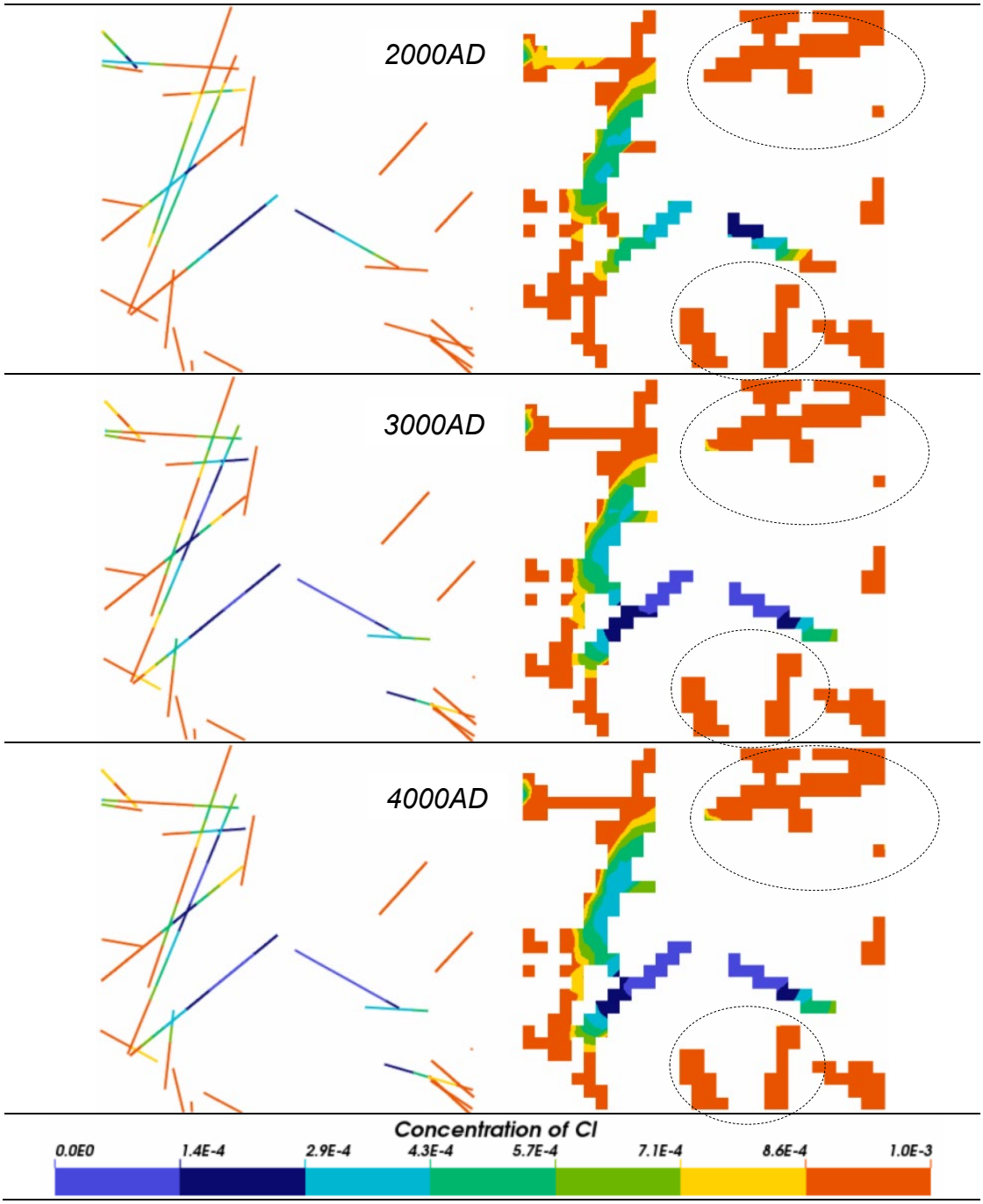

Figure 5-6. *Concentration (mass fraction) of chloride ions for a horizontal slice through the SFL model at −490m depth. Three points in time are displayed and calcite reactions are included in all calculations. The images to the left use the DFN representation and those on the right use the ECPM representation (elements with permeability less than $1x10^{-17}m^2$ are not shown). Note that some upscaled elements seem to be permeable where there are no fractures (indicated by "circles" in dashed-lines). This is because the fractures are just above or below the 2D slice taken here.*

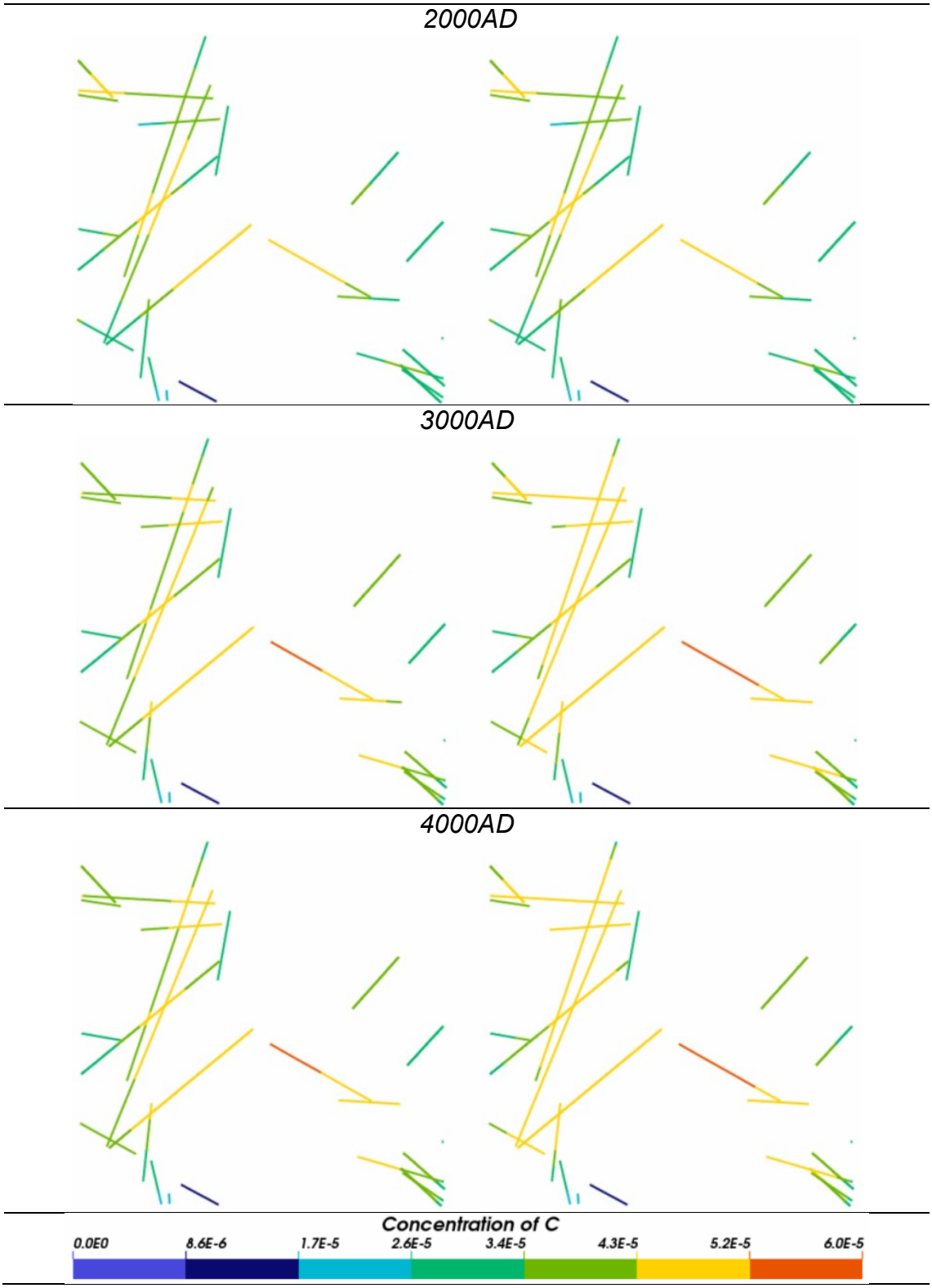

Figure 5-7. *Concentration (mass fraction) of inorganic carbon for a horizontal slice through the SFL model at −490m depth. Three points in time are displayed for the DFN representation. The images on the left include the effect of chemical reactions and those on the right do not.*

The behaviour of carbon is very different when compared with the behaviour of chloride ions. The carbon concentration appears to increase towards the centre of the model as time passes, which is the reverse of the behaviour witnessed for the chloride ions. The reason for this is simply that the initial carbon concentration is higher at shallow depths and this is brought down to repository depth by the ingress of meteoric water.

The effect of the calcite reactions is also apparent in Figure 5-8. Without these reactions, there are much larger carbon concentrations in the repository fracture water than if the reactions are included.

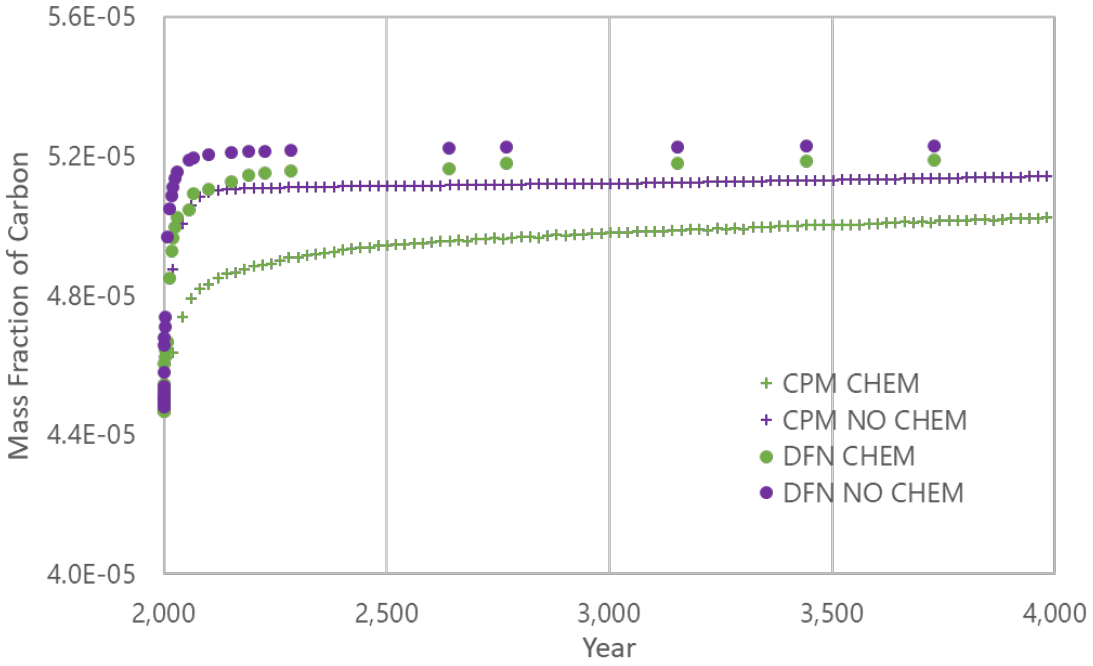

Figure 5-8. *Concentration of inorganic Carbon at a point within the repository area as a function of time for calculations using DFN/ECPM representations and with/without chemical reactions.*

6 ENABLING LARGER CALCULATIONS VIA PARALLELISATION

6.1 Implementation

The algorithms within ConnectFlow are highly efficient, allowing models with billions of finite elements to be processed on a single CPU. The central principle of the algorithm is to divide the calculation into stages. In the first stage, every fracture is discretised using two dimensional finite elements and the response of the fracture to different combinations of boundary conditions is calculated. This process is carried out for all fractures in isolation. The response functions for the fractures are then used to generate an equation for the global system. The global problem is then solved. A schematic of the process is shown in Figure 6-1 and a more detailed description of the numerical techniques is provided in (Wood 2018).

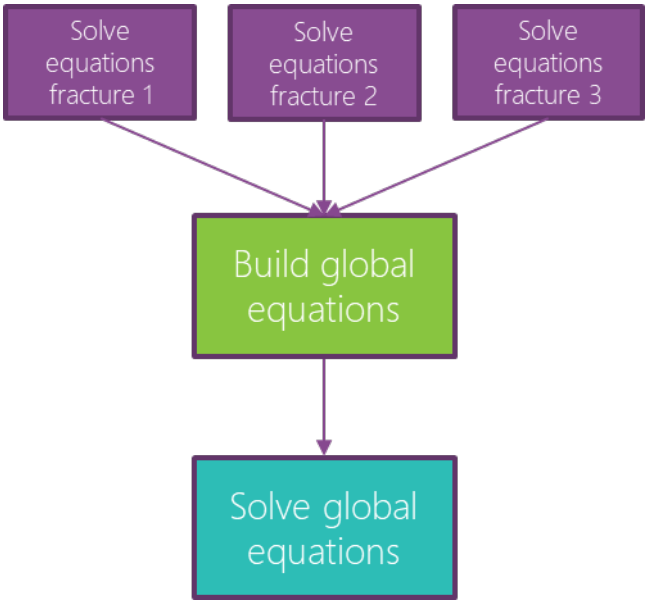

Figure 6-1. *DFN calculations in ConnectFlow are carried out in stages. In the first stage known as the "fracture solve" a series of calculations are carried out on each fracture individually. Next the "fracture solve" calculations are use to build up the global equations. Finally, the global equations are solved, which is known as the "global solve".*

Despite the efficiency of the ConnectFlow algorithms, transient calculations involving the transport and reaction of multiple species are computationally challenging. Significant effort has therefore been made to improve the performance of ConnectFlow calculations via parallelisation and other techniques.

As noted above, the first stage of ConnectFlow calculations (Figure 6-1) is carried out on each fracture separately. This part of the calculation is readily parallelised, since groups of fractures can be processed on different CPU cores with minimal communication. This part of the calculation is also the most time consuming and will provide the biggest gain in performance from parallelisation. This "fracture solve" has been parallelisation in ConnectFlow using the Message Parsing Interface (MPI). This is a distributed memory parallelisation specification that is widely used within the scientific computing community.

Building the global equations can also be time-consuming. This has been optimised so that it is not a bottleneck in the calculations (roughly two orders of magnitude speed up has been obtained).

ConnectFlow uses an external library developed by the Lawrence Livermore National Laboratory, known as Hypre, to solve the global equations (LLNL, 2017). This library is a collection of linear solvers and preconditioners, optimised for parallel calculations. Experience has shown that the most robust solver is the GMRES (with restart) incorporating an ILU preconditioner (known as Euclid within the Hypre library). However, this solver often will not parallelise for (typical) calculations involving large variations in transmissivity and transport aperture. The algebraic multigrid preconditioner (known as BoomerAMG) often has a much better parallel scaling for real-world flow and transport calculations. Unfortunately, for coupled calculations of the type carried out in the previous chapters, it has not been robust enough to use. Consequently, coupled calculations have been carried out, in serial, using GMRES with an ILU preconditioner. Single variable calculations have been carried out using the BoomerAMG preconditioner (in parallel where possible).

Figure 6-2 shows a performance benchmark using a nonlinear flow calculation for a large DFN. The DFN is an SFL site-scale model involving 1.9 million fractures and 5.9 million fracture tessellates. The newly parallelised fracture calculation shows good scaling, with a factor of 20 reduction in calculation time on 32 processors compared to 1 processor. The global solve is carried out using the BoomerAMG preconditioner and shows some parallel scaling. The calculation time reduced by a factor of about 7 on 32 processors compared to 1 processor.

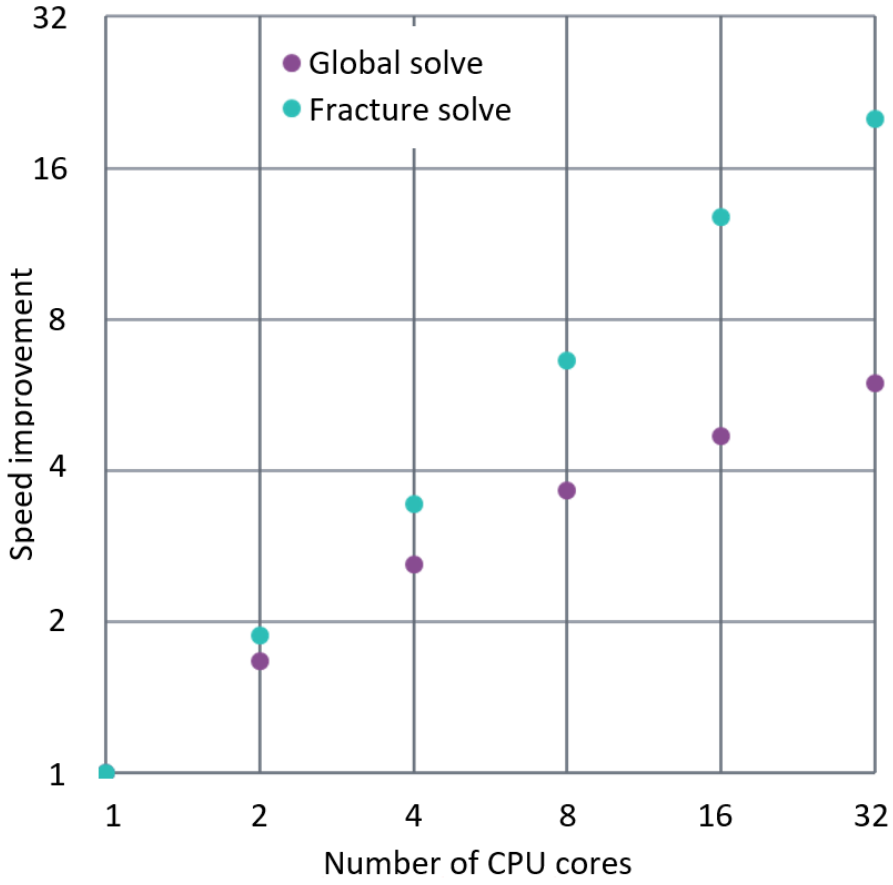

Figure 6-2. *Benchmark for a nonlinear SFL site scale model. The "fracture solve" has been parallelised and scales well with the number of CPU cores. The "global solve" uses the BoomerAMG preconditioner from the Hypre library. This has some parallel scaling in this example.*

6.2 Olkiluoto

Parallelisation has two main benefits. Firstly, employing parallelisation for a calculation allows it to be completed more rapidly. For example, the Olkiluoto model presented in in Section 2 required around 16 days of simulation time. Running the calculation in parallel (on 32 cores) provided a solution in less than 2 days. Secondly, with the parallelised code it is possible to attempt larger calculations than would be possible in a reasonable timescale on a single CPU. The parallelisation has allowed the investigatation of two more complex variants of the Olkiluoto model. The first variant covers a larger simulation domain and includes smaller fractures. The second variant includes five reference waters instead of just two.

6.2.1 Variant A

Figure 6-3 shows two simulation domains relative to Olkiluoto island. The darker grey box is the original "baseline" simulation domain while the lighter grey box is the simulation domain used for Variant A. The latter includes more of the coastal region where discharges might occur. The area of the Variant A simulation domain is 2.7 x 3.0 km, an increase of 43%.

The baseline model includes fractures greater than 20 m in size in a sub-section of the domain immediately around the repository. In the rest of the domain, fractures greater than 200 m in size are included. Variant A includes fractures greater than 20 m in the entire domain. This change, combined with the extended domain, means there are far more fractures in Variant A compared to the baseline model. Variant A has 538,000 fractures and 1,776,000 sub-fractures, compared to 29,000 fractures and 461,000 sub-fractures in the baseline model. The differences between the baseline model and Variant A are summarised in Table 6-1.

Figure 6-4 shows the concentration of saline water at 4000 AD on horizontal cross sections through the two models at repository depth. The fracture network used in the baseline model is very sparse when when compared with Variant A. The effect of the additional fractures and larger simulation domain on the saline concentration is significant, particularly for larger fractures and deformation zones and the smaller fractures that surround them.

Table 6-1. *Key differences between the baseline model and Variant A.*

Property	Baseline	Variant A
Simulation domain	2.7 x 2.1 km	2.7 x 3.0 km
Fracture sizes included	> 20 m around repository > 200 m elsewhere	> 20 m everywhere
Number of fractures	29,000	538,000
Number of sub-fractures	461,000	1,776,000

Consider the large fracture highlighted at the bottom right of the baseline model (Figure 6-4). This appears to be a significant conduit for meteoric water to travel to repository depth (it is located beneath a surface location with a relatively high elevation on Olkiluoto island). Consider also the two fractures highlighted to the top left, these provide a path for saline water to be displaced and rise to the surface near the coastline. The equivalent fractures in Variant A have much larger variations in salinity, suggesting they have a more significant impact on the transport in this model. This is probably because the additional fractures and larger simulation domain in Variant A allows solutes to infiltrate, percolate and discharge more readily.

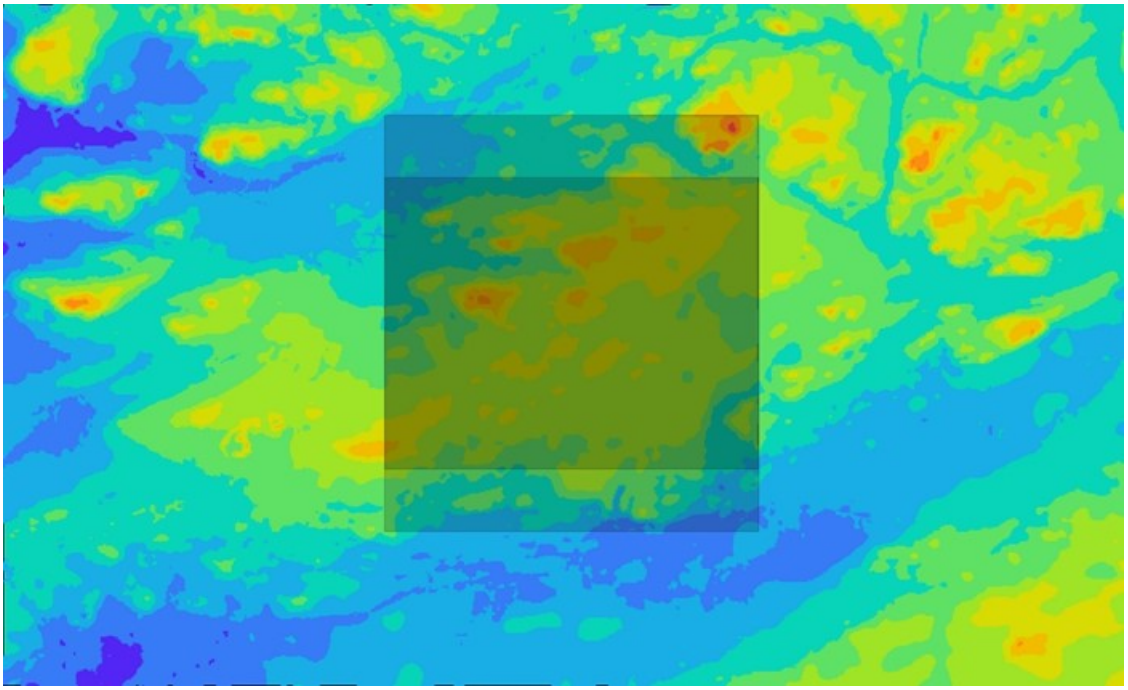

Figure 6-3. *Topography of Olkiluoto island with blues representing the sea. The baseline domain (dark grey) and Variant A domain (light grey) are also shown.*

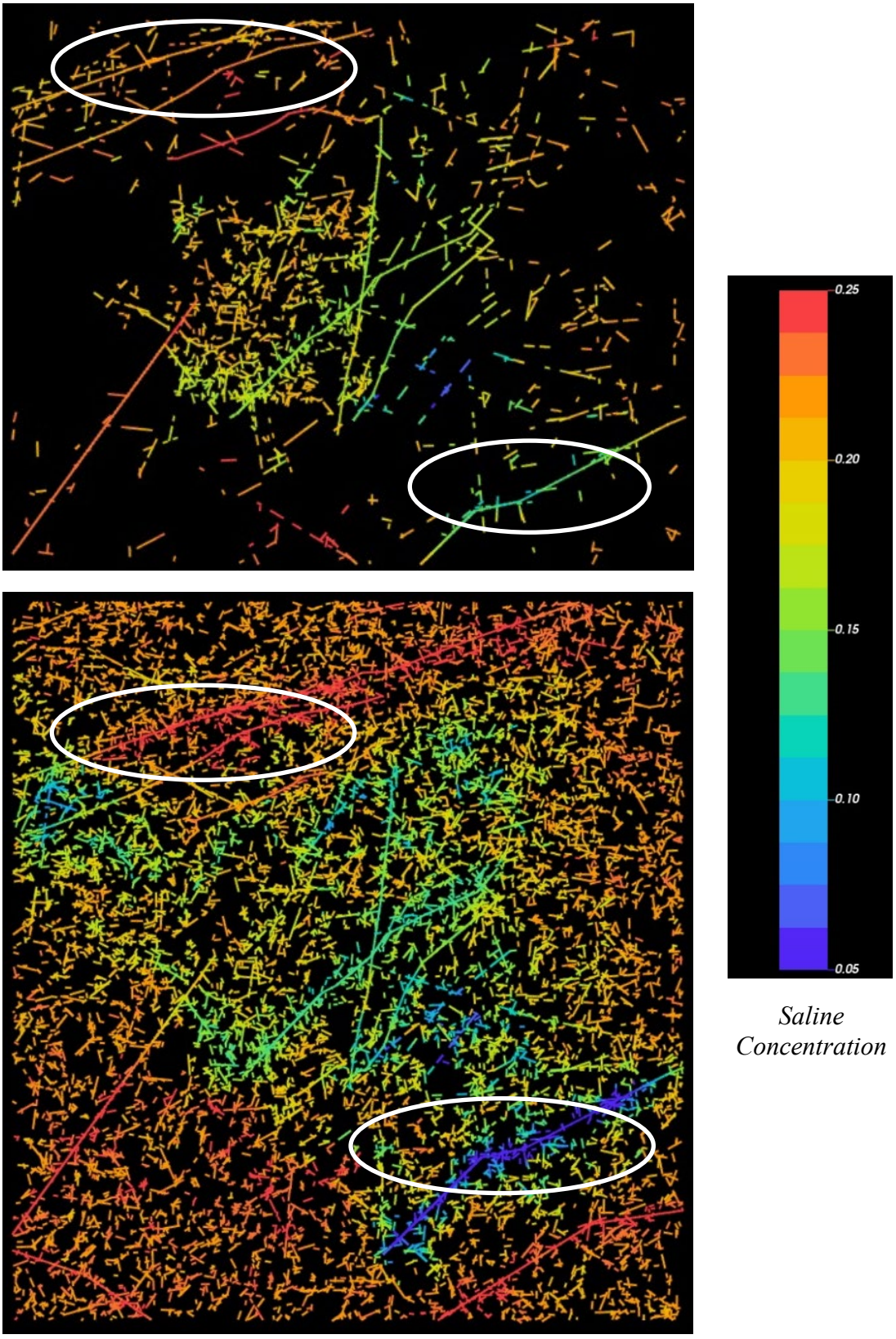

Figure 6-4. *Horizontal cross-section of saline concentration at repository depth at 4000 AD. The baseline model is at the top and Variant A is at the bottom. Equivalent fractures are highlighted in each.*

6.2.2 Variant B

The baseline model considers the mixing of two reference waters: saline water, and meteoric water. The saline water is resident at depth and is slowly displaced by meteoric water infiltrating into the top of the model. The actual groundwater compositions at Olkiluoto are much more complex than specified in that simple model. In the Site Descriptive Model (SDM - Partamies and Pitkänen 2014), five distinct reference waters are specified. Conceptually, these reference waters reflect important aspects of changes in the climate and evolution of the hydrogeological conditions.

- Brine: representing ancient water found at depth, characterised by high salinity and high chloride content (> 20,000 mg/L) of non-marine origin.
- Littorina: representing Littorina and Baltic Sea water.
- Meteoric: representing water of meteoric origin, chemically altered by infiltration though the ground surface.
- Glacial: representing glacial melt water, characterised by significantly depleted $\delta^{18}O$ levels.
- Subglacial: representing ancient water, composed of meteoric and brackish waters from periods before the Weichselian glaciation.

In Variant B, the evolution of groundwater composition at Olkiluoto is formulated in terms of transport equations for fractions of these five reference waters. Transport is conservative (without reactions). The chemical composition of reference water is detailed in Table 6-2. In all other regards, Variant B is identical to the baseline model.

At the present day, these reference waters are arranged roughly in layers with brine mostly restricted to depths below the repository. Sub-glacial waters are the highest concentration at repository depth with glacial waters residing mostly above this. A mixture of Littorina and meteoric waters form the next layer with meteoric water infiltrating through the ground surface. As time progresses it is expected that the meteoric water will displace and dilute the reference waters below it.

Figure 6-4 and Figure 6-5 show concentrations of these five different waters within a horizontal slice at repository depth, calculated at 2000 AD and 4000 AD. The concentration of meteoric water at this depth increases with time in most locations; particularly the centre of the model and the bottom right of the model. It decreases in one of the larger fractures to the top left, displaced from below by an increasing brine and sub-glacial concentration. Glacial and Littorina concentrations increase over time in several of the larger fractures at this depth and appear to move into some of the smaller fractures. Concentrations in the large fracture to the bottom right decrease, displaced by meteoric water from above. Sub-glacial concentrations decrease with time in the centre of the model, displaced by glacial/Littorina waters. Sub-glacial concentrations also decrease to the bottom right, displaced by meteoric waters, but increase slightly to the top left. Brine concentrations increase with time at the top left of the model, displacing meteoric water. Brine concentrations reduce to the centre of the model, displaced by glacial/Littorina waters. Brine concentrations also reduce to the bottom right of the model, displaced by meteoric water.

Table 6-2. *Chemical compositions of the five reference waters considered at Olkiluoto.*

Chemical	**Brine**	**Littorina**	**Meteoric**	**Glacial**	**Subglacial**
TDS (g/L)	68.8	11.9	0.5	0.0	4.9
Cl (g/L)	43.000	6.500	0.060	0.001	3.000
HCO3 (g/L)	0.012	0.093	0.291	0.000	0.013
SO4 (g/L)	0.001	0.890	0.048	0.001	0.001
Mg (g/L)	0.002	0.448	0.016	0.000	0.027
Br (g/L)	0.348	0.022	0.000	0.000	0.021
$\delta^{2}H$ Ratio	−49.8	−37.8	−82.1	−166.0	−86.0
$\delta^{18}O$ Ratio	−10.1	−4.7	−11.5	−22.0	−12.0
Na (g/L)	9.750	3.674	0.025	0.000	1.350
K (g/L)	0.022	0.134	0.007	0.000	0.005
Ca (g/L)	15.700	0.151	0.092	0.000	0.510

Variants A and B are the largest calculations that have been attempted in the current work. In future we hope to simulate even larger models that also include reactive transport. This will require:

- Implementation of more efficient & parallelisable solvers
- and/or a more robust approach to sequential iteration.

Alternatively, if the coupling between salinity and pressure is ignored, then these calculations are probably already feasible.

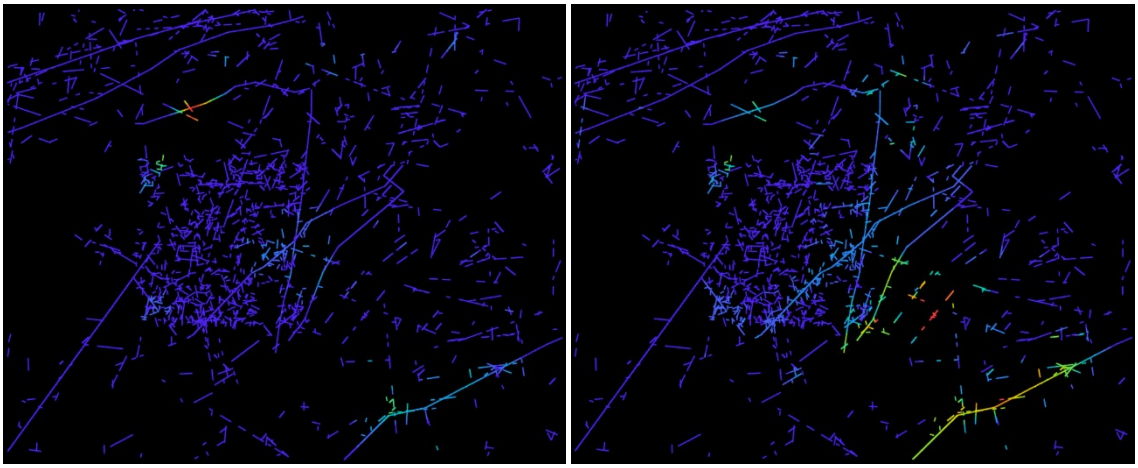

Meteoric 2000AD | Meteoric 4000AD

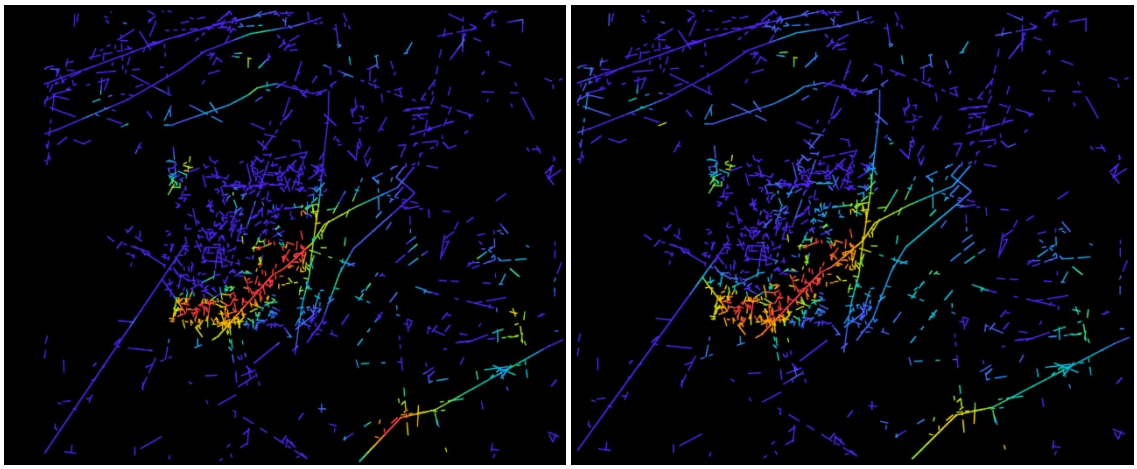

Littorina 2000AD | Littorina 4000AD

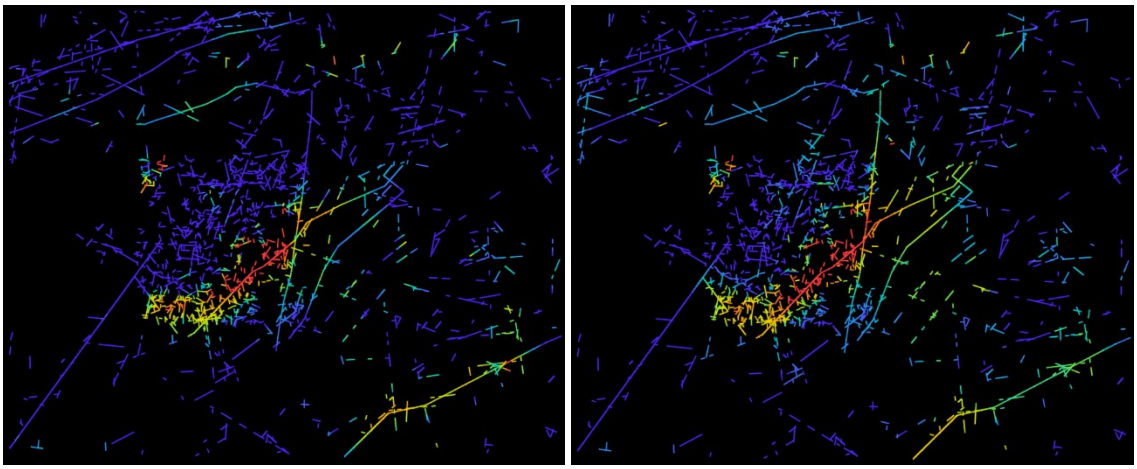

Glacial 2000AD | Glacial 4000AD

Figure 6-5. *Concentrations of three reference waters at 2000 AD and 4000 AD on horizontal slices at repository depth. Note, the colour scales are not consistent between different reference waters.*

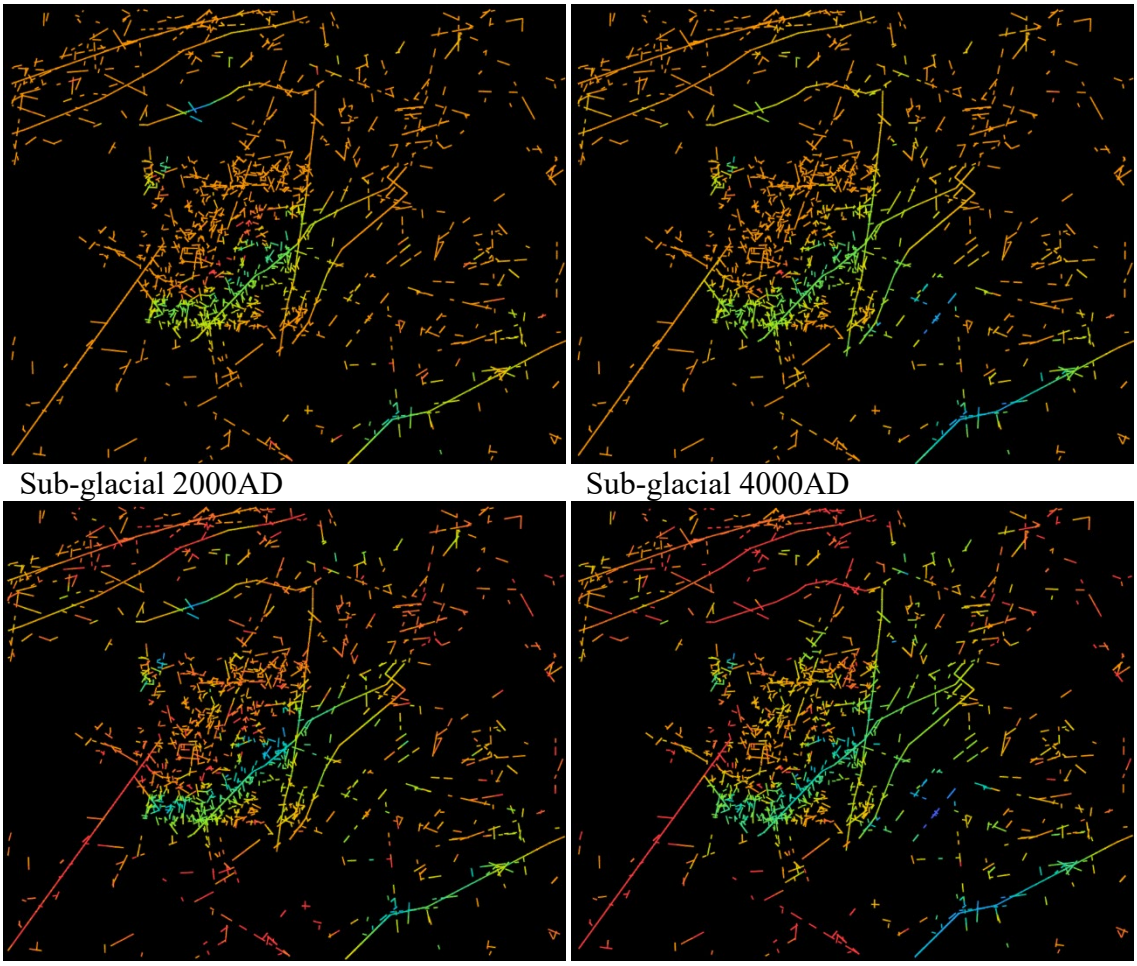

Sub-glacial 2000AD | Sub-glacial 4000AD

Brine 2000AD | Brine 4000AD

Figure 6-6. *Concentrations of two reference waters at 2000 AD and 4000 AD on horizontal slices as repository depth. Note, the colour scales are not consistent between different reference waters.*

7 CONCLUSIONS

In this report, an important new methodology for modelling hydrogeochemical evolution within fractured crystalline rock has been presented. The approach taken is to extend the discrete fracture network (DFN) facility for the ConnectFlow groundwater flow and transport software to explicitly model hydrogeochemical processes. This has involved four major improvements to the software specific to DFN models:

(i) A new finite volume algorithm for modelling solute diffusion into the pore space of the rock surrounding each fracture (i.e. matrix diffusion).

(ii) An updated set of transport algorithms to solve the advection-diffusion equation for multiple solute species rather than just a single species (which is fully coupled to the pressure solution via the buoyancy term in Darcy's equation). This new implementation also enables the viscosity and density to be a function of temperature, pressure and salinity, where previously the viscosity was constant and the density was only a function of salinity.

(iii) A new interface to the iPhreeqc geochemical library. This enables chemical reactions between solutes and with minerals (which coat the fractures and/or the rock pores) to be calculated.

(iv) A substantial portion of the ConnectFlow DFN groundwater flow and transport algorithms have been parallelised to improve performance.

These developments have been verified using single fracture and/or random fracture test cases by comparing them with ECPM calculations and analytical solutions. Single fracture tests have shown exact matches between DFN and two-dimensional CPM calculations. Results from random fracture tests show some differences between the DFN and ECPM representations, but these differences reduce as the resolution of the ECPM increases. These tests also show good agreement with analytical solutions.

In addition to simple verification calculations, four sets of larger, repository-based calculations have been presented:

(i) Site-scale calculations of meteoric water ingress at Olkiluoto using the original implementation of DFN salt transport in ConnectFlow and a finite volume rock matrix diffusion algorithm. This calculation effectively involves two reference waters (saline and meteoric). Meteoric water ingress is clearly observed at repository depth over the 2000 year timescale of the calculations.

(ii) Site-scale calculations of meteoric water ingress at Olkiluoto using the new multi-solute DFN salt transport algorithm in ConnectFlow and the new rock matrix diffusion algorithm. This calculation also involves two reference waters (saline and meteoric). The new salt transport implementation results in a similar rate of ingress of meteoric water compared to (i) above.

(iii) Site-scale calculations of meteoric water ingress at Olkiluoto using five reference waters. These results are consistent with the results in (ii) above and show more detail regarding the origin and destination of the five reference waters.

(iv) Repository-scale calculations of meteoric water ingress at SFL using multi-solute DFN salt transport, rock matrix diffusion and calcite reactions via the iPhreeq interface. This calculation involves the transport of six chemical species (C, H, O, Ca, Cl and Na) and three chemical tracers (pH, pe and charge balance). Freshwater ingress and calcite precipitation are clearly observed over the 2000 year timescale of the calculations.

In all cases, comparisons to ECPM calculations are presented. These have a very high resolution to provide the best approximation of a DFN. ECPM calculations used for safety cases would not necessarily use such a high resolution for two reasons. Firstly, because the ECPM approximation typically overestimates flow and underestimates travel times, which is usually conservative in an assessment context. This effect will typically be more pronounced for a lower resolution ECPM. Secondly, a lower resolution makes the calculations more tractible. The DFN and ECPM calculations always show qualitative agreement but the exact quantitative results differ because of the upscaling approximations. Explicit DFN calculations allow these differences to be quantified.

The hydrogeochemical DFN calculations presented in this report are computationally challenging. The parallelisation of the code has significantly improved performance, but some challenges remain. The strong coupling between the pressure and salt concentration in the calculations have prevented the use of sequential iteration in any of the larger models presented (including those for the ECPM models) and all variables have been solved simultaneously. One exception to this, which may be useful for future calculations, has been the SFL ECPM calculations where a 'hybrid' approach is taken. Here the pressure is solved at the same time as the solutes with the highest mass fraction (Na, Cl and Ca) while those with lower mass fractions (H, C, O and E) are solved sequentially. This approach takes advantage of the fact that the lower mass fraction solutes have less influence on groundwater density and so can be solved separately from the pressure.

The BoomerAMG preconditioner was found to be insufficiently robust for these coupled calculations while the ILU preconditioners typically did not parallelise. Further work is required to find an appropriate solver that is robust, efficient and parallelises for these problems.

The SFL and Olkiluoto calculations in this report have used similar boundary conditions. A fixed (Dirichlet) concentration is applied over each face of the model and a fixed pressure is also applied on the top surface of the model. Lateral boundaries have a no-flow condition applied. Future developments may provide more realistic top boundary conditions that allow concentration, recharge and discharge to vary with time (where appropriate).

The initial concentration within the SFL and Olkiluoto models is interpolated from lower resolution ECPM site-scale models. Consistent steady state pressures are calculated and used as an initial condition for the transient calculation. This approach has limitations since the concentrations within a DFN would be expected to show much larger spatial variations between fractures than could be extracted from the ECPM site scale models. This means the transient DFN calculations typically show rapid transient behaviour to start with before slowing down. A methodology for implementing appropriate initial conditions will need to be developed.

The explicit representation of reactive transport within discrete fracture network models is a significant advance that allows groundwater flow, transport and hydrogeochemical reactions to be properly represented in a fractured bedrock. The calculations presented here have shown that DFN similations provide qualitatively similar results to those obtained from an ECPM representation with sufficiently high resolution. The ECPM is a more indirect approach, however, and differences do exist between the results from the DFN and the ECPM representations. These differences are expected to reduce as the resolution of the upscaling is increased.

REFERENCES

Carrera J, Sánchez-Vila X, Benet I, Medina A, Galarza G and Guimerà J, 1998. On matrix diffusion: formulations, solution methods and qualitative effects. Hydrogeology Journal 6, Pages 178–190.

Charlton S R and Parkhurst D L, 2011. Modules Based on the Geochemical Model PHREEQC for Use in Scripting and Programming Languages. Computers & Geosciences.

Follin S, 2008. Bedrock hydrogeology Forsmark. Site descriptive modelling, SDM-Site Forsmark. SKB R-08-95, Svensk Kärnbränslehantering AB.

Hartley, L, Appleyard P., Baxter, S., Hoek, J., Roberts, D., & Swan, D. 2012a. Development of a Hydrogeological Discrete Fracture Network Model of Olkiluoto; Site Descriptive Model 2011. Working Report 2012-32. Posiva Oy, Eurajoki.

Hartley L, Hoek J, Swan D, Appleyard P, Baxter S, Roberts D, Simpson T, 2013. Hydrogeological modelling for assessment of radionuclide release scenarios for the repository system 2012. Posiva Working Report 2012-42, Posiva Oy, Finland.

Hartley, L, Hoek J, Swan D, Baxter S, Woollard H, 2012b. Hydrogeological Discrete Fracture Modelling to Support Rock Suitability Classification. Posiva WR-2012-48.

Hartley L and Joyce S, 2013. Approaches and algorithms for groundwater flow modeling in support of site investigations and safety assessment of the Forsmark site, Sweden. Journal Of Hydrology, 500, 200–216. doi:10.1016/j.jhydrol.2013.07.031.

Hoch A R and Jackson C P, 2004. Rock-matrix diffusion in transport of salinity. Implementation in CONNECTFLOW. SKB R-04-78, Svensk Kärnbränslehantering AB.

Hoek J, Hartley L and Baxter S, 2016a. Hydrogeological Modelling for the Olkiluoto KBS 3H Safety Case. Posiva WR-2016-21.

Hoek J, Hartley L, Joyce S, Marsic N, Crawford J, Sidborn M, 2016b. Modelling Hydrogeochemical Evolution for the Olkiluoto KBS-3H Safety Case. Posiva WR-2016-11.

Joyce S, Applegate D, Appleyard P, Gordon A, Heath T, Hunter F, Hoek J, Jackson P, Swan D, Woollard H, 2014a. Groundwater flow and reactive transport modelling in ConnectFlow. SKB R-14-19, Svensk Kärnbränslehantering AB.

Joyce S, Simpson T, Hartley L, Applegate D, Hoek J, Jackson P, Swan D, Marsic N, Follin S, 2010. Groundwater flow modelling of periods with temperate climate conditions – Forsmark. SKB R-09-20, Svensk Kärnbränslehantering AB.

Joyce S, Woollard H, Marsic N, Sidborn M, 2014b. Future evolution of groundwater composition at Forsmark during an extended temperate period. SKB R-14-26, Svensk Kärnbränslehantering AB.

Kestin J, Khalifa E, Correia R, 1981. Tables of the dynamic and kinematic viscosity of aqueous NaCl solutions in the temperature range 20–150 °C and the pressure range 0.1–35 MPa. Journal of Physical and Chemical Reference Data 10, 71.

LLNL, 2017. Hypre Users Manual, Release 2.11.2. Lawrence Livermore National Laboratory.

Löfgren M, Sidborn M, 2010. Statistical analysis of results from the quantitative mapping of fracture minerals in Forsmark. Site descriptive modelling – complementary studies. SKB R-09-30, Svensk Kärnbränslehantering AB.

Löfman J and Karvonen T, 2012. Simulations of Hydrogeological Evolution at Olkiluoto. Posiva WR-2012-35.

Neretnieks I, 1980. Diffusion in the rock matrix: an important factor in radionuclide retardation? Journal of Geophysical Research 85(B8), Pages 4379–4397.

Parkhurst D L and Appelo C, 1999. User's guide to PHREEQC (Version 2)—A computer program for speciation, batch-reaction, one-dimensional transport, and inverse geochemical calculations:.U.S. Geological Survey Water-Resources Investigations Report 99–4259.

Partamies and Pitkänen, 2014. Mass-balance modelling results of groundwater data collected at Olkiluoto over the period 2004 - 2007. Working Report 2014-6. Posiva Oy. Finland.

Posiva, 2009. Olkiluoto Site Description 2008. Posiva 2009-01, Posiva Oy, Finland.

Posiva, 2011. Olkiluoto Site Description 2011. Posiva 2011-02, Posiva Oy, Finland.

Posiva, 2012a. Safety Case for the Disposal of Spent Nuclear Fuel at Olkiluoto. Synhesis 2012, Posiva Oy, Finland.

Posiva, 2012b. Nuclear Waste Management at Olkiluoto and Loviisa Power Plants: Review of Current Status and Future Plans for 2013-2015. YJH-2012. Posiva Oy, Finland.

Posiva, 2015. Modelling Hydrogeochemical Evolution for the Olkiluoto KBS-3H Safety Case. Posiva Oy, Finland.

Salas J, José Gimeno M, Auqué L, Molinero J, Gómez J, Juárez I, 2010. SR-Site – hydrogeochemical evolution of the Forsmark site. SKB TR-10-58, Svensk Kärnbränslehantering AB.

Sidborn M, Marsic N, Crawford J, Joyce S, Hartley L, Idiart A, Manuel de Vries L, Maia F, Molinero J, Svensson U, Vidstrand P, Alexander R, 2014. Potential alkaline conditions for deposition holes of a repository in Forsmark as a consequence of OPC grouting. SKB R-12-17, Svensk Kärnbränslehantering AB.

Sigg L, 2000. Redox potential measurements in natural waters: significance, concepts and problems. In Schüring J, Schulz H D, Fischer W R, Böttcher J, Duijnisveld W H M (eds). Redox: fundamentals, processes and applications. Berlin: Springer, 1–12.

SKB, 2011a. Long-term safety for the final repository for spent nuclear fuel at Forsmark. SKB TR-11-01, Svensk Kärnbränslehantering AB.

SKB, 2011b. RD&D programme 2010, SKB TR-10-63, Svensk Kärnbränslehantering AB.

SKB, 2013. Summary of discrete fracture network modelling as applied to hydrogeology of the Forsmark and Laxemar sites, SKB R-12-04, Svensk Kärnbränslehantering AB.

SKB, 2016. SFL - Groundwater flow and reactive transport modelling of temperate conditions, SKB R-19-02, Svensk Kärnbränslehantering AB.

Smellie J, Pitkänen P, Koskinen L, Aaltonen I, Eichinger F, Waber F, Sahlstedt E, Siitari –Kauppi M, Karhu J, Löfman J, Poteri A, 2012. Evolution of the Olkiluoto Site: Palaeohydrogeochemical Considerations. Posiva WR-2014-27.

Sudicky and Frind, 1982. Contaminant Transport in Fractured Porous Media: Analytical Solutions for a System of Parallel Fractures. Water Resources Research Vol. 18, No. 6, Pages 1634-1642.

Trinchero P, Román-Ross G, Maia F, Molinero J, 2014. Posiva Safety Case Hydrogeochemical Evolution of the Olkiluoto Site, Posiva Working Report. 2014-09, Posiva Oy.

Wood, 2018. ConnectFlow Technical Summary, Release 12.0. Wood.